

Drive System Selection and Simulation for a Humanoid

Damien Kee

19th October 2001

28 Penaton St.
Corinda Qld 4075
Ph (07)3379 5378
s369472@student.uq.edu.au

19th October 2001

Prof. Simon Kaplan
Head of School of Information Technology
and Electrical Engineering
University of Queensland
St. Lucia Qld 4072

Dear Professor Kaplan,

In accordance with the requirements of the degree of Bachelor of Engineering (Hons), I present the following thesis entitled "*Drive System Selection and Simulation for a Humanoid*". This work was performed under the supervision of Dr Gordon Wyeth.

I declare that the work submitted in this thesis is my own, except as referenced, and has not been previously submitted for a degree at the University of Queensland or any other institution.

Yours Sincerely,

Damien Kee

Acknowledgements

I would like to thank a few people for the help and support they have provided throughout the year.

- Gordon Wyeth, my supervisor, for his advice and encouragement throughout the year. His friendliness, approachability in all matters, and fantastic Lego set, made for an enjoyable year. His ability to organise and manage such a large group of riff raff undergraduates is a sight to behold.
- All the guys in the Lab for making it such a fun place to work, especially at 2:00am in the morning. The impromptu arguments, soccer matches and debates livened up even the most dull of days.
- Iilan, Mark Venz and David Prasser for their help with all things unix
- Andrew Smith, Mark Wagstaff, Andrew Blower and Mark Venz for the great conversations we had over end-of-week beers.
- Skye, Nick, Ang, Margo, Raelene and Ana for keeping me sane and reminding me of my life outside of engineering.
- My parents for their continuing support of everything I do.

The following paper, *Design of an Autonomous Humanoid Robot*, by Wyeth, Kee, Wagstaff et al. was accepted at the Australian Conference on Robotics and Automation, Sydney 2001.

Design of an Autonomous Humanoid Robot

Gordon Wyeth, Damien Kee, Mark Wagstaff, Nathaniel Brewer,
Jared Stirzaker, Timothy Cartwright, Bartek Bebel
School of Computer Science and Electrical Engineering
University of Queensland
St. Lucia, Queensland, 4072
Australia

Abstract

This paper describes the design of an autonomous humanoid robot. The robot itself is currently under construction, however the process of designing the robot has revealed much about the considerations for creating a robot with humanoid shape. The mechanical design is a complete CAD solids model, with specific motors and transmission systems selected. The electronic design of a distributed control system is also complete, along with the electronics for power and sensor processing. A high fidelity graphical simulator has been developed, providing important early feedback on critical design decisions.

1 Introduction

There are several reasons to build a robot with humanoid form. It has been argued that to build a machine with human like intelligence, it must be embodied in a human like body. Others argue that for humans to interact naturally with a robot, it will be easier for the humans if that robot has humanoid form. A third, and perhaps more concrete, reason for building a humanoid robot is to develop a machine that interacts naturally with human spaces. The architectural constraints on our working and living environments are based on the form and dimensions of the human body. Consider the design of stairs, cupboards and chairs; the dimensions of doorways, corridors and benches. A robot that lives and works with humans in an unmodified environment must have a form that can function with everyday objects. The only form that is guaranteed to work in all cases is the form of humanoid.

1.1 The *GuRoo* Project

The *GuRoo* project in the University of Queensland Robotics Laboratory aims to design and build a 1.2m tall robot with human proportions that is capable of balancing, walking, turning, crouching, and standing from a prostrate position. The target mass for the robot is 30 kg, including on-board power and computation. The robot will have active, monocular, colour vision and vision processing.

The intended challenge task for the robot is to play a game of soccer with or against human players or other humanoid robots. To complete this challenge, the robot must be able to move freely on its two legs. It requires a

vision sense that can detect the objects in a soccer game, such as the ball, the players from both teams, the goals and the boundaries. It must also be able to manipulate and kick a ball with its feet, and be robust enough to deal with legal challenges from human players. Clearly, the robot must operate in a completely autonomous fashion without support harnesses or wiring tethers.

These goals are yet to be realised for the *GuRoo* project. Currently the robot exists as a complete mechanical CAD model (see Figure 1), a complete electronic model and a high fidelity dynamic simulation. The dynamic simulation has been programmed to crouch, jump and balance. The progress to this stage has revealed much about the design considerations for a humanoid robot.

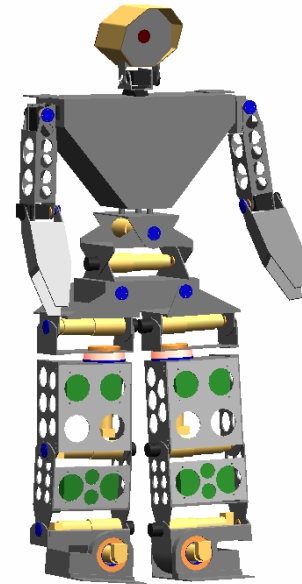


Figure 1: Full CAD model of the *GuRoo* humanoid robot.

1.2 Paper Overview

This section has described the motivation for building a humanoid robot, and the specific challenge that has been set for the *GuRoo* project. The subsequent section will look at other humanoid robot projects, including bipedal walking robots.

The rest of the paper describes the mechanical, electronic and software design of the *GuRoo* robot. In

particular, the paper will detail the mechanical model of the robot and a comparison to the human form, the motors and sensors, the complete electronic design, a full dynamic software simulation of the robot, the software architecture of the robot, and results for balancing and crouching in simulation.

2 Prior Art

2.1 Bipedal Walking Robots

Research into bipedal walking robots can be split into two categories: *active* and *passive*. The passive or un-powered category (for example, McGeer’s passive dynamic walker [McGeer, 1990]) is of interest as it illustrates that walking is fundamentally a dynamic problem. Passive walkers do not require actuators, sensors, or computers in order to make them move, but walk down gentle slopes generating motion by the hardware geometry. The passive walkers also illustrate the walking can be performed with very little power input.

Active walkers can further be split into two categories; those that employ the natural dynamics of specialised actuators, and those that are fully power operated. Raibert [Raibert, 1986] and later Pratt [Pratt, 1998] have shown some impressive feats of walking and gymnastic ability in robots that have the capacity for energy storage in the actuator. These robots have been shown to have robust and stable performance from relatively simple control mechanisms.

The alternate approach is to control the joints through pre-specified trajectories to a known “good” gait pattern (for example, [Golden, 1990]). This is a simple approach, but lacks robustness to disturbances. This approach becomes more complex when additional layers are added to provide adjustments to the gait for disturbance. Controlling a fully powered biped in a manner that depends on the dynamic model is complicated by the complex dynamic equations for the robot’s motion. Yamaguchi et al. [Yamaguchi, 1998] moved a dynamic torso with significant mass through 2 DOF to keep the Zero Moment Point (ZMP) within the polygon of the support foot. This approach contributed to successful control of the robot, but produces an awkward gait.

2.2 Bipedal Walking Humanoid Robots

There are few examples of autonomous biped walkers that resemble the structure of a human. The Honda company biped robots, P2 and P3 are two of the few examples of such robots [Hirai, 1998]. P3 can walk on level ground, walk up and down stairs, turn, balance, and push objects. The robot is completely electrically and mechanically autonomous. The Sony SDR-3X robot is another example with similar capabilities, although details of the design are yet to be published.

3 Mechanics

The mechanical design of the humanoid requires careful and complex tradeoffs between form, function, power, weight, cost and manufacturability. For example, in terms of form, the robot should conform to the proportions of a

1.2m tall human. However, retaining the exact proportions compromises the design in terms of the selection of actuation and mechanical power transmission systems. Affordable motors that conform to the dimensional restrictions have insufficient power for the robot to walk or crouch. This section describes the final mechanical design and how the balance between conflicting design requirements has been achieved.

3.1 Proportions

The target proportions for the robot are based on biomechanical data of the human form. Figure 2 shows the proportions of the frontal plane dimensions of a 50th percentile male based on data from a United States survey [Dempster, 1965]. The dimensions shown in millimetres indicate the appropriate sizes of anatomical features when scaled to a total height of 1200 mm against the comparable dimensions on GuRoo.

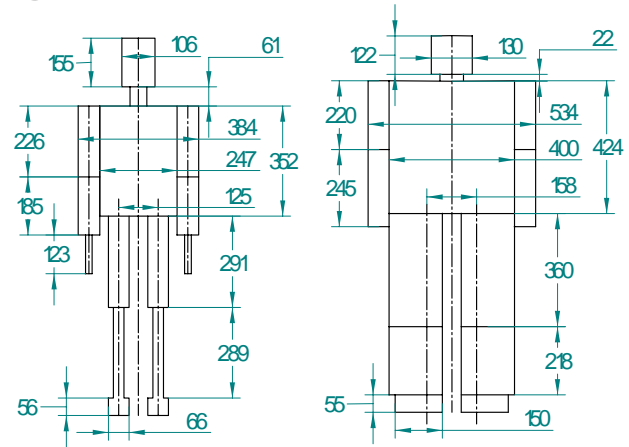


Figure 2: The proportions of typical human anatomy compared to the matching proportions of GuRoo’s anatomy. The dimensions indicate the sizes for a human scaled to 1.2m in height.

By comparison, GuRoo is somewhat thickset in the legs, as was dictated by the form of the chosen actuators (see Section 3.3). The spacing between the hips and ankles has been retained, rather than placing the hips and ankles along the frontal centreline of each leg. Our simulation studies showed that the required torques around the roll axes of the hips and ankles becomes excessive if the hips and ankles are spaced too far apart (see Section 5.3).

The body and upper leg of GuRoo are somewhat longer than the counterparts in the human model. This is due to the chain of actuators required for three degrees of freedom in the waist and hips respectively (see Section 3.2). Consequently, the lower leg and the neck and head are shorter to compensate. The overall effect is still convincingly human-like in shape.

The changes in volume required to house the actuators, as well as the mass of the actuators themselves have an effect on the mass distribution. Table 1 shows the mass distribution of GuRoo compared to that of a human. The most notable exception is that the shin and foot are much heavier in GuRoo than the human counterpart, due to the mass of the powerful actuators required in the ankle. The arms are significantly lighter than the human

counterpart, as they are significantly inferior in power and do not have hands. GuRoo's mass distribution is closer to the human distribution than either MIT's active bipedal walker [Paluska, 2000], or McGeer's passive dynamic bipedal walker.

Table 1: Comparison of GuRoo mass distribution with human mass distribution, and with the mass distribution of MIT's M2 bipedal walker and McGeer's passive dynamic walker.

Body Component	GuRoo mass (kg)	GuRoo	Human	M2	PDW
Head and Upper torso	7.3	24%	31%	0%	0%
Abdomen and Hips	9.1	30%	27%	51%	50%
Thigh	5.8	19%	20%	22%	30%
Shin and Foot	6.4	21%	12%	27%	20%
Arm	1.9	6%	10%	0%	0%
Total	30.5				

The other notable point from Table 1 is the total mass of the robot. A 1.2 m tall human would typically be a child approaching his or her 7th birthday, with a 50th percentile mass of 23 kg. A child with mass of 30.5 kg at the same age would be in 97th percentile, indicating that GuRoo is somewhat overweight.

3.2 Architecture

The extent to which human joint function can be replicated is another key factor in robot design. Figure 3 shows the degrees of freedom contained in each joint area of the robot. In the cases where there are multiple degrees of freedom (for example, the hip) the joints are implemented sequentially through short links rather than as spherical joints. Other key differences to the human form are the lack of a continuous flexible spine, and the lack of a yaw axis in the ankle. Another point to note is that the roll and pitch axes of the ankle are orthogonal, whereas the human ankle has an angle of about 64° between the roll and pitch axes.

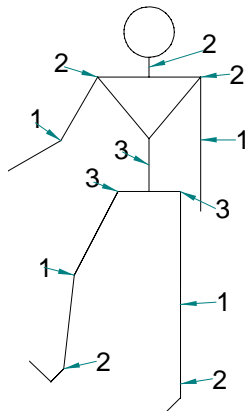


Figure 3: The location of the joints in GuRoo, indicating the degrees of freedom in each joint.

3.3 Motor Choice

The key element in driving the mechanical design has been the choice of actuator. The robot has 23 joints in total. The legs and abdomen contain 15 joints that are required to produce significant mechanical power, most generally with large torques and relatively low speeds. The other 8 joints drive the head and neck assembly, and the arms. The torque and speed requirements are significantly less. Factors of cost, weight and availability limited the choice of actuators to rotary DC motors

The 15 high power joints all use the same motor-gearbox combination. The motor is a Maxon RE 36 wound for a nominal voltage of 32V. This motor can provide 88.5 mNm of torque continuously, with a matching current consumption of 1.99 A. The motor has a maximum permissible speed of 8200 RPM. The gearbox has a reduction of 156, with an efficiency of 72%. The maximum continuous generated output torque is 10 Nm, with a maximum output speed of 51 RPM, or 5.3 rad/s. The thermal limits of the motor permit intermittent output torque of up to 19Nm. Each motor is fitted with an optical encoder for position and velocity feedback. The total mass of the motor/gearbox/encoder unit is 0.85 kg.

The 8 low power joints are Hi-Tec RC servo motors model HS705-MG. These motors have an integrated gearbox and have rated output torque to 1.4 Nm, at speeds of 5.2 rad/s. These also have potentiometer feedback and built-in control and power electronics. They require 6V power, and a pulse width modulated signal to indicate desired position. The mass of each unit is 0.125 kg.

4 Electronics

A distributed control network controls the robot, with a central computing hub that sets the goals for the robot, processes the sensor information, and provides coordination targets for the joints. The joints have their own control processors that act in groups to maintain global stability, while also operating individually to provide local motor control. The distributed system is connected by a CAN network. In addition, the robot requires various sensor amplifiers and power conversion circuits.

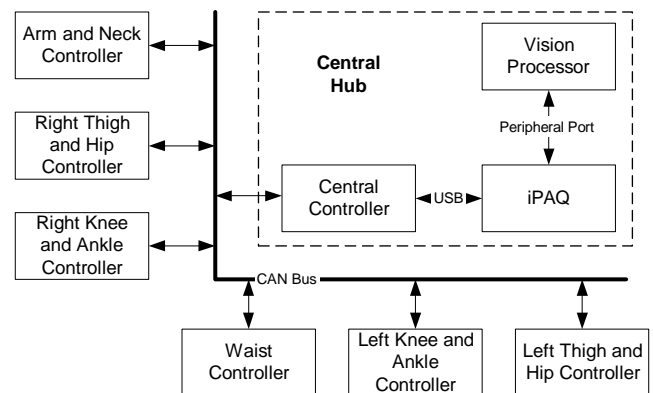


Figure 4: Block diagram of the distributed control system.

4.1 Computing

4.1.1 Central Hub

The central control of the robot derives from a hub of three heterogeneous microprocessors that provide coordination between joints, integrate sensor information, and process the vision input. This hub also provides communication to the outside world through user interfaces and communication peripherals.

The primary component of the central controller is an iPAQ pocket pc from Compaq. The iPAQ features a 208 MHz StrongARM microcontroller, 32 Mb of RAM and a 320 x 240 colour screen. The screen is touch sensitive allowing stylus input of text and graphics. The iPAQ has 16 Mb of Flash ROM to store the operating system. The iPAQ in the GuRoo operates with Windows CE. As well as the touch screen interface, the iPAQ is equipped with a speaker and microphone, a joystick, and four push-buttons. It has an infra-red interface for external communication.

The second component of the central hub is a TMS320F243 microcontroller that acts as an adapter and filter for the robot's internal CAN network (see Section 4.1.3). The microcontroller communicates with the robot's distributed control system through the CAN network, and to the iPAQ through the iPAQ's USB serial communication port. The microcontroller also manages the power supply (see Section 4.2.3) providing centralised control of the robot power supply in the event of system failure. This microcontroller is the same device used in the joint controllers (see Section 4.1.2).

The final component of the central is the vision processing board. This board has been developed for the ViperRoos robot soccer team [Chang, 2001] and features a 200 MHz Hitachi Super-H SH4 microcontroller, an FPGA-based programmable camera and bus adapter, 16 Mb of RAM, 8 Mb of flash ROM, and 512 kb of fast SRAM for video caching. The board interfaces to the 100 pin parallel peripheral bus on the iPAQ to provide real time visual display on the iPAQ's colour screen. The vision input comes from a custom digital CMOS camera, based around the OV7620 camera chip from OmniVision, which can provide 640 x 480 images at up to 25 fps. The camera can provide data in YUV or RGB formats, and can be programmed to only send data from selected areas of the sense region.

4.1.2 Joint Controllers

The TMS320F24x series is a 32 bit DSP designed for motor control. The availability of the Control Area Network (CAN) module in this series, along with bootloader programmable internal Flash memory makes the device particularly attractive for this application. Furthermore the device features 8k words of internal flash memory, 8 PWM channels with deadband generation, quadrature input circuitry, an 8 channel 10 bit analog to digital converter with a conversion time of 800ns, a power drive protection external interrupt, and a 50ns instruction time. The TMS320F241 from Texas Instruments operates at 20MHz, and can read the A/D converter, calculating a PID control law, current limit, and generate the required PWM output, in under 10 μ s [Wyeth, 2001]. In this application, we use the TMS320F243, which has an

external bus that is used for attaching additional sensor interfaces. Five controller boards control the 15 high power motors, each board controlling three motors. A sixth controller board controls the eight RC servo motors.

4.1.3 Internal Network

The CAN bus is a highly reliable standard developed by Robert Bosch GmbH for use in the automotive environment. It is a multi-master system, with sophisticated error checking and arbitration, so that any high priority message will always get through first without corruption by other messages. All data contained in each packet (up to eight bytes) is also checked with a Cyclic Redundancy Check (CRC) error-checking scheme that can correct up to five random errors, and will be automatically retransmitted if not correct. The network operates at up to 1 Mbit/sec.

4.2 Power

4.2.1 Drive Power Electronics

The drive power electronics is based on a switch mode power stage, requiring only a single supply rail and having an efficiency over 90%. This efficiency results in several advantages such as small size, lower cost power devices and less heatsinking. The H-Bridge channels are driven from separate PWM outputs of the DSP, allowing the deadband features of the PWM peripheral to be used, along with the immediate (<12ns) shutdown of these pins in the event of a fault which triggers the Power Drive Protect Interrupt (PDPInt) pin on the DSP.

A integrated solution was chosen for this design – the SGS-Thomson L6203. This device uses low on-resistance and fast switching MOSFETs, to give maximum efficiency and best control. The voltage limit of the devices is 48V, and the total continuous RMS current limit is 4A. This is a good match to the chosen motors and batteries. The total on-resistance of the power devices is 0.3 Ω . The cost of the device is low, compared to a discrete solution, and the volume and mass of the electronics is minimised by the choice of an integrated solution.

4.2.2 Battery Packs

The power for the 15 high power motors is provided by 4 x 1.5Ah 42V NiCd packs. These packs are effectively paralleled to a common bus (see Section 4.2.3). The packs are chosen to give 20 minutes of continuous operation. The power for the 8 low power motors is derived from a single 3Ah 7.2 V NiCd battery pack. The power for the control electronics is derived from a second single 3Ah 7.2V NiCd pack. The voltage from this pack is distributed to the various boards that require power where it is regulated locally.

4.2.3 Power Regulation

Connecting NiCd batteries in parallel can be extremely hazardous to the life of the batteries. Uneven charging and discharging characteristics between packs can lead to uneven load sharing and high current circulation between packs. The power from each pack is controlled through switch mode buck converters to provide even current sharing between packs, providing a voltage bus at marginally below the lowest battery voltage.

4.3 Sensing

4.3.1 Joint Sensing

Current sensing is performed in the high power joints by a 0.01Ω resistance in the ground leg of the H-Bridge. The voltage from these sense resistors is amplified by differential amplifiers and measured by the ADC. Current is also checked against a screwdriver adjustable hard limit that is used to trigger the Power Drive Protect interrupt. The position feedback from the encoders on the high power joints provides a count on every edge of both quadrature channels. This provides 2000 counts per motor revolution from the 500 count encoder wheels. In addition, each DSP can measure the bus voltage, and the temperatures of the MOSFETs and motors.

4.3.2 Motion Sensing

In addition to the sensing in each joint, and of course the visual feedback, the robot features 2 x 2-axis accelerometers to provide information about the torso's dynamic behaviour and the relationship to the vertical gravity force. While it is impossible to resolve the motion components of the body's acceleration from the effects of gravity, these sensors may be able to provide information with regard to disturbances while walking – playing a similar role to the human middle ear.

Provision has also been made for the contact switches in the feet and in the joints. These switches may prove useful for determining when contact is made with the ground, or initialising joints at robot start up.

5 Software

The software consists of four main entities: the global movement generation code, the local motor control, the low-level code of the robot, and the simulator. The software is organised to provide a standard interface to both the low-level code on the robot and the simulator. This means that the software developed in simulation can be simply re-compiled to operate on the real robot. Consequently, the robot needs a number of standard interface calls that are used for both the robot and the simulator. Figure 5 shows modularisation of the software, and the common interfaces.

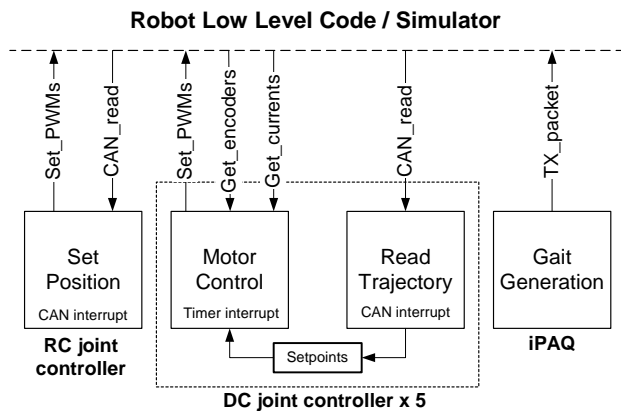


Figure 5: Block diagram of common software modules and the interface used to both the real robot and the simulator.

5.1 Simulator

At present, all evaluations of the robot have taken place in a high fidelity dynamic simulator. The simulator is based on the *DynaMechs* project [McMillan, 1995]. *DynaMechs* is an object-oriented, open source code library that provides full dynamic simulation for tree-structured robots having a star topology. The algorithms are capable of simulating fixed and mobile bases. The library is based on efficient recursive algorithms for the dynamic calculations, and provides graphical display of the robot in an OpenGL environment.

The simulator uses the *DynaMechs* package as the core, with additions to simulate specific features of the robot such as the DC motors and motor drives, the RC servos, the sensors, the heterogeneous processing environment and the CAN network. These additions provide an identical interface between the dynamic graphical simulation and the controller and gait generation code. The parameters for the simulator are derived from the CAD models and the data sheets from known components. These parameters include the modified Denavit-Hartenberg parameters that describe the robot topology, the tensor matrices of the links and the various motor and gearbox characteristics associated with each joint. The surface data from the CAD model is also imported to the simulator for the graphical display.

The simulator uses an integration step size of $500\mu\text{s}$ and updates the graphical display every 5ms of simulated time. When running on 1.5 GHz Pentium 4 under Windows 2000, the simulation updates all 23 joints at a very useable 40% of real time speed.

5.2 Joint Controller Software

For the high power DC motor joints, the simulator provides the programmer with readings from the encoders and the current sensors, based on the velocities and torques from the dynamic equations. In the case of the RC servos, the simulator updates the position of the joints based on a PD model with a limited slew rate. The programmer must supply the simulator with PWM values for the motors to provide the control. The simulator provides fake interrupts to simulate the real events that are the basis of the control software.

There are two types of joint controller boards used in the robot – five controller boards control the fifteen high power motors and one controller controls the eight low power motors. The controller software for the low power motors is a single interrupt routine that is triggered by the arrival of a CAN packet addressed to the controller's mailbox. The routine reads the CAN mailbox for the change in position sent by the gait generation routine. The PWM duty cycle that controls the position of the RC servos is varied accordingly.

The control loop for the high power controllers has two interrupt routines. As for the low power controller, an interrupt is executed upon receipt of trajectory data in the CAN mailbox. The data is used to set the velocity setpoints for the motor control routine. There is also a periodic interrupt every $500\mu\text{s}$ to run the motor control software. The motor control routine compares the error between velocity setpoint and the encoder reading and generates a PWM value for the motor based on a Proportional-Integral control law. The routine also checks

the motor current against the current limits, and adjusts the PWM value to prevent over-current situations.

5.3 Motion Generation Software

To this point, the software for motion generation has been used to test the designed geometries and chosen motors in the simulator. The software uses only local joint feedback; it does not use feedback from the joint sensors in a global sense or use the motion sensors to modify the motion to maintain balance. The tests are run without current limiting in the local control loop to evaluate worst-case performance.

The first test motion is a crouch with a return to the standing position. This test has been designed to evaluate the required torques in the pitch joints of hip, knee and ankle. The worst-case results for the knee joint are shown in Figure 6. The second test motion is a lean to balance over one leg, designed to evaluate the required torques in the roll joints of hip and ankle. The joints are driven according to the following equations. The worst-case results for the ankle are shown in Figure 7. In both of these worst cases, the current consumption only briefly exceeds the continuous current rating, and the motor stays within thermal limits.

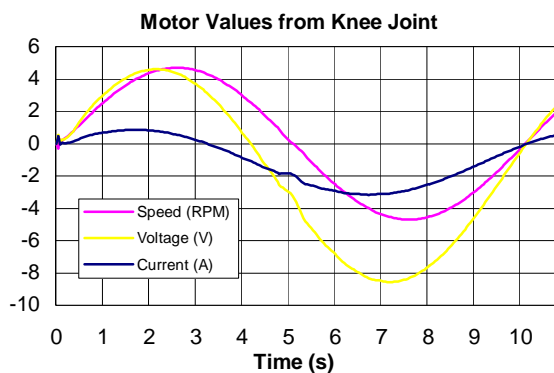


Figure 6: Simulation results for knee motor during a squatting movement. The movement cycle time is 10 seconds.

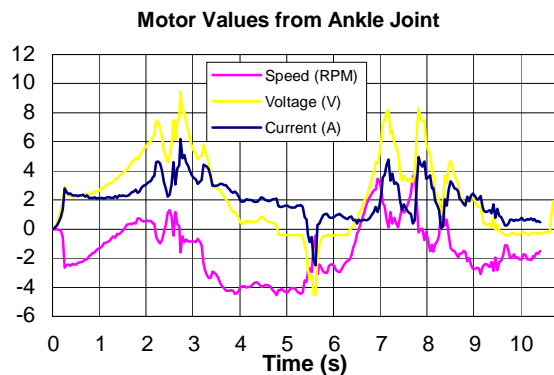


Figure 7: Simulation results for ankle motor during a balancing movement. The movement cycle time is 10 seconds.

6 Conclusions

This paper has illustrated the design of a practical,

affordable, autonomous, humanoid robot. The robot is well proportioned in relation to the human form, with most of the major degrees of freedom of the human body implemented. The robot design has a distributed control design with processors dedicated to each of the key roles around the robot. Investigations of the CAD design using a high fidelity simulation have shown that robot is capable of crouching and balancing.

[**Note for reviewers:** This project involves a large team who intend to have the real robot constructed and walking by September. The final paper will have further results, and the conference presentation is likely to feature a video, and possibly the robot itself.]

References

- [Chang, 2001] M. Chang, B. Browning and G. Wyeth. ViperRoos 2000. RoboCup-2000: Robot Soccer World Cup IV. Lecture Notes in Artificial Intelligence 2019. Springer Verlag, Berlin, 2001.
- [Dempster, 1965] W.T.Dempster and G.Gaughran. Properties of body segments based on size and weight. American Journal of Anatomy, 1965.
- [Golden, 1990] J. A. Golden and Y. F. Zheng. Gait Synthesis For The SD-2 Biped Robot To Climb Stairs. International Journal of Robotics and Automation 5(4). Pages 149-159, 1990.
- [Hirai, 1998] K. Hirai, M. Hirose, Y. Haikawa, and Takenaka. The Development of Honda Humanoid Robot. IEEE Conference on Robotics and Automation, 1998.
- [Hodgins, 1995] J. K. Hodgins, W. L. Wooten, D. C. Brogan, and J. F. O'Brien. Animating Human Athletics. In Computer Graphics, (Siggraph 1995).
- [McMillan, 1995] S. McMillan, Computational Dynamics for Robotic Systems on Land and Underwater, PhD Thesis, Ohio State University, 1995.
- [McGeer, 1990] T. McGeer. Passive Dynamic Walking. International Journal of Robotics Research, 9(2):62-82, 1990.
- [Paluska, 2000] D.J. Paluska, Design of a Humanoid Biped for Walking Research, Masters Thesis, MIT, 2000.
- [Pratt, 1998] J. Pratt and G. Pratt. Intuitive Control of a Planar Bipedal Walking Robot. IEEE Conference on Robotics and Automation, 1998.
- [Raibert, 1986] M. H. Raibert. Legged Robots that Balance. MIT Press, Cambridge, MA, 1986.
- [Wyeth, 2001] Wyeth G.F., Kennedy J. and Lillywhite J. (2000) Distributed Digital Control of a Robot Arm, Proceedings of the Australian Conference on Robotics and Automation (ACRA 2000), August 30 - September 1, Melbourne.
- [Yamaguchi, 1998] J. Yamaguchi, S. Inoue, D. Nishino, and A. Takanishi. Development of a Bipedal Humanoid Robot Having Antagonistic Driven Joints and Three DOF Trunk. Proceedings of the 1998 IEEE/RSJ Conference.

Abstract

This thesis details the selection and simulation of a drive system for a bi-ped humanoid robot, dubbed the GuRoo. The limiting factor for many years in the field of humanoid robotics, has been finding and implementing actuators that are powerful enough yet at the same time light enough to allow autonomous bi-pedal walking.

Different actuation methods are considered and a final decision of a combination of Servo motors and Brushed DC motors was chosen. Limited information was available for the Servo motors chosen, and as such only basic evaluation of their characteristics is given. Comprehensive characteristics of the DC motor / gearhead combination is presented, along with a brief outline of the mechanical implementation of the actuators.

The simulation section outlines the development of an accurate humanoid model file, and its incorporation in the DynaMechs simulation package. Two anthropomorphic movements, Crouching and Standing on One Leg, are implemented and the suitability of the actuators evaluated. The implementation of a spring on two joints, to aid the actuators, was necessary and its design and effect on the robot discussed. From the preliminary results obtained from the simulator, it is possible to see that the GuRoo is capable of walking.

Currently a complete mechanical CAD model exists for the GuRoo and is being constructed. The project is awaiting delivery of the actuators, but it is hoped by the end of the year a set of legs can be constructed and tested.

Contents

1	Introduction	1
1.1	Introduction	1
1.2	RoboCup	1
1.3	Drive Systems	2
1.4	Legged Movement	2
1.5	Achievements	2
1.6	Thesis Outline	3
2	Previous Research	5
2.1	Pistons	6
2.1.1	Hydraulics	6
2.1.2	Pneumatics	6
2.2	Artificial Muscles	6
2.2.1	Air Muscles	7
2.2.2	Muscle Wire	7
2.3	DC Motors	8
2.3.1	Stepper Motors	8
2.3.2	Servo Motors	8
2.3.3	Linear Actuators	9
2.4	Power transmission	9
2.4.1	Pulleys	9
2.4.2	Gearhead	10
2.5	Feedback	12
3	Specifications	13
3.1	The GuRoo	13
3.2	Drive System Specifications	13

3.2.1	Electro-Mechanical Design	13
3.2.2	Power	14
3.2.3	Actuator Control	14
3.3	Design considerations	14
3.3.1	Degrees of Freedom	14
3.3.2	Actuator type	14
4	Initial Humanoid Design	16
4.1	Humanoid Model	16
4.2	Mechanical Design	17
4.3	Motor Selection	17
4.3.1	Upper Body	17
4.3.2	Lower Body	20
4.3.3	Gearhead Selection	22
4.3.4	Motor Unit Characteristics	22
4.4	Distributed Ball Joint	25
4.5	Power Transfer	26
4.6	Pulleys	26
5	Actuator Simulation	29
5.1	Simulator	29
5.2	DM file Structure	29
5.3	mDH parameters	31
5.4	Coordinate Frames	31
5.5	Inertia Tensors	32
5.6	Z screw Link	33
5.7	Actuator Types	33
6	Simulation Results	35
6.1	Crouching	35
6.2	Standing on One Leg	38
6.3	Spring Implementation	40
6.4	Modelling the Spring	41
6.5	Spring Implementation	43

7 Conclusion	45
7.1 Further Work	45
A Humanoid .dm file	51
B Motor / Gearhead Characteristic Spreadsheet	60
C Standing on One Leg Graphs	61
D Coordinate Frames	65
E Maxon Datasheets	70

List of Figures

1.1	Commercially available quadrapod and hexapod [17]	3
2.1	(l-r) Honda's Asimo, Sony's SDR-3X	5
2.2	Pneumatic piston [7]	6
2.3	Air Muscle from the Shadow Robot Group	7
2.4	Muscle wire actuated hexapod[20]	7
2.5	(l-r) Linear Positioning System from Lintech[16] and Linear Actuators on INRA's humanoid BIP[4]	9
2.6	Standard Pulley arrangement[11]	10
2.7	Spur Gear cut-away	11
2.8	2 Stage Planetary Gear head cut-away	11
2.9	Harmonic drive operation[12, modified].	12
4.1	Location and Degrees of Freedom Within the GuRoo	17
4.2	Final CAD design	18
4.3	Hitec HS-705MG used in the Upper Body	19
4.4	Initial Servo calculation.	19
4.5	Location of Servo Motors	20
4.6	Complete Motor / Gearbox / Encoder Combination	20
4.7	Initial Crouching Movement	21
4.8	Location of the Brushed DC motors in the Lower Body	23
4.9	Ball and Socket Joint	25
4.10	(l-r) Distributed Hip and Spine Joints	26
4.11	Boss and End Cap Assembly with Maxon Motor	27
4.12	Initial Pulley Design	27
5.1	Upper Leg Coordinate frame	32
5.2	Current Simulator Graphics Model	34

6.1	Crouch Simulation	35
6.2	Motor Torques for initial Crouch movement	36
6.3	Motor Torques for modified crouch	37
6.4	Standing on One Leg Simulation	38
6.5	Time line of Standing on One Leg Movement	39
6.6	Selected Motor Torques for Standing on One Leg movement	40
6.7	Spring / Motor combination	40
6.8	Spring Implementation	41
6.9	One Degree of Freedom simulator model	42
6.10	Spring Torque based on theoretical spring constant	42
6.11	Spring Torque based on estimated spring constant	43
6.12	Selected Motor Torques with Spring Implementation	44
7.1	Lower Leg link in progress.	46

List of Tables

4.1	Location and Degrees of Freedom	16
4.2	Motor Specifications	21
4.3	Gearhead / Encoder Specifications	22
6.1	Crouch Parameters	36
6.2	Standing on One Leg joint times and angles	39

Chapter 1

Introduction

1.1 Introduction

The task of designing and building an anthropomorphic robot, dubbed the ‘GuRoo’ (Grossly Underfunded Roo) was undertaken by 12 undergraduate students. The project was split into software, hardware and electromechanical sub-teams and then further divided into specialised thesis topics. This thesis outlines the drive system for a bi-ped humanoid robot, from design through to simulation. The overall aim of the University of Queensland’s Humanoid project is to compete in the humanoid league division of the annual Robocup Competition.

1.2 RoboCup

The RoboCup concept was first conceived in 1992 after a Workshop on Grand Challenges in Artificial Intelligence was held in Japan. From this workshop, the concept of an annual robotics competition based on the sport of soccer was proposed. Soccer was chosen as the competition sport, due to the large research possibilities from the field and the global appreciation of the sport. The first official competition was held in Paris 1998, with the participation of universities and research centres around the world. The vision set down by the RoboCup organisers is:

By the year 2050, develop a team of fully autonomous humanoid robots that can win against the human world soccer champions[23].

Whilst the technology does not currently exist to realise this vision, it is hoped that through the competition, and the subsequent sharing of information, it will be possible

by 2050.

1.3 Drive Systems

The drive system of a robot is the means by which it moves. Mobile robots historically have been actuated by wheels or treads. The drive system is often seen as the keystone to any mobile robotics problem. The selection of the actuators influences almost all aspects of the complete robot, including the mechanical design, power system and control system. The mechanical structure is dependent on the size and shape of the actuators and the weight influences the structural design. The choice of actuators also influences the power system of the robot, often with the need to isolate the power electronics from the digital electronics. This choice will also affect the choice and parameters of any control system.

1.4 Legged Movement

Mobile robotics up to the present day predominantly uses wheels for actuation, a more robust and easily implemented solution than legs. The push towards legged robots has emerged due to the desired for robots to work independently, in more unstructured and hostile environments. Terrains requiring a solution other than wheels are common, but the coordination and actuation of legged robots has proved difficult, with six-legged (hexapod) and four legged (quadrapod) robots enjoying the most success. The main benefit available to quarapods and hexapods is the ability to have a stable base of three or more legs at any point during its gait. The bi-ped design has been avoided up until recently, due to the complex stability issues associated with bi-pedal locomotion.

It has been argued that the best form of a robot to interact with humans is a robot of human form, and thus the purpose behind the design and construction of a humanoid, is to as closely model the appearance and mobility of a human as possible.

1.5 Achievements

This thesis does not specifically set out to choose a set of actuators for a humanoid robot, rather it outlines the procedure undertaken for the selection, simulation and evaluation of the actuators required for a mobile robotics application. Possible solutions and the factors used in determining the best solution for the GuRoo are put forward, followed by the simulation and evaluation of the actuators eventually chosen.

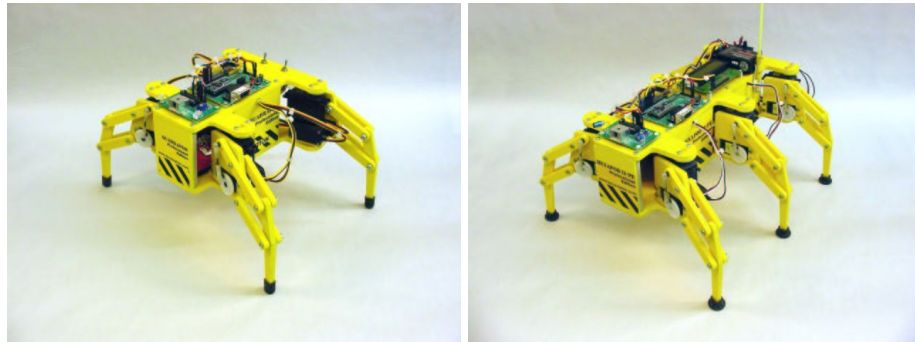


Figure 1.1: Commercially available quadrupod and hexapod [17]
With gaits allowing 3 legs to be in contact with the ground at all times, these legged robots are very stable.

The GuRoo drive system selected was a combination of Hitec HS-705MG servo motors and Maxon RE36/GP42 brushed DC motor / planetary gearhead combination. The results from the DynaMechs simulation package prove that the motors selected are adequate for a crouch and standing on one leg movement. The gait implementation results by Smith[25] show that they are also adequate for static walking.

1.6 Thesis Outline

Chapter 2 outlines the current technology in actuation devices for small scale robotic applications. It provides advantages and disadvantages of each, as well as a financial and maintenance cost.

Chapter 3 covers the broad aims and objectives of the GuRoo project and the specific requirements of the Drive system.

Chapter 4 presents the actuators chosen, and their characteristics. The electromechanical design associated with the location and implementation of the actuators is also provided.

Chapter 5 comprehensively describes the modelling of the robot and actuators within the DynaMechs simulator.

Chapter 6 provides the results and analysis of two common human movements, crouching and standing on one leg.

Chapter 7 concludes the thesis and provides scope for further work with the humanoid drive system.

Chapter 2

Previous Research

Due to the relative new field of legged robots, there are relatively few humanoid projects in the world, The most publicly known being Asimo and SDR-3X from Honda[2] and Sony[26] respectively. The majority of humanoid projects throughout the world use geared DC motors, but there are a few other options worth considering.

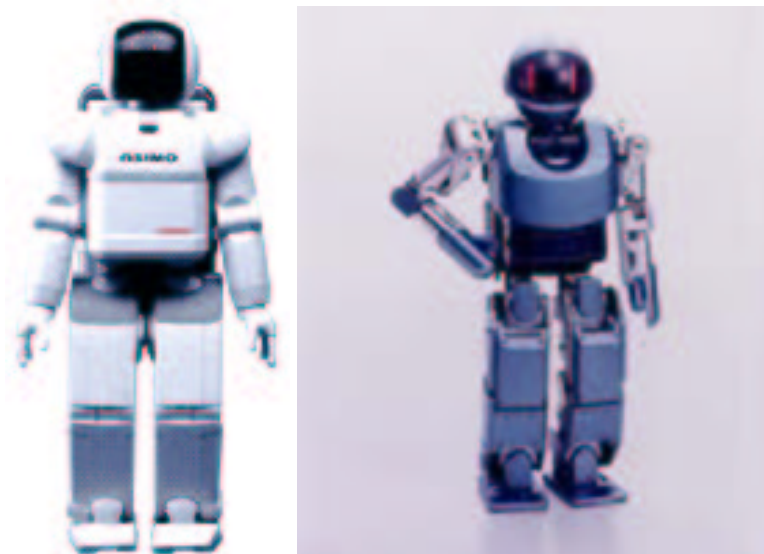


Figure 2.1: (l-r) Honda's Asimo, Sony's SDR-3X

2.1 Pistons

2.1.1 Hydraulics

Hydraulics are a relatively old technology, that rely on a flow of pressurised fluid to propel a piston along a shaft. By varying the volume and flow rate of this fluid, it is possible to obtain accurate position and velocity control. Hydraulics are capable of transmitting large amounts of force along a relatively small flow line. Flow rate and direction is usually controlled by solenoid activated valves. Hydraulics are evident in large heavy machinery and as such are not popular with mobile robotics. They require however, a lot of ancillary equipment, including a means of pressurising and storing fluid to run[7, 10].

2.1.2 Pneumatics

Pneumatics are a sub group of hydraulics that are actuated by air pressure. The benefit this gives is the ability to source and exhaust the required air from the atmosphere, negating the need for a fluid sump. Control of pneumatics is quite difficult due to the compressibility of air.



Figure 2.2: Pneumatic piston [7]

2.2 Artificial Muscles

Artificial muscles are based closely on human muscles, with the elongated device contracting like a muscle when actuated.

2.2.1 Air Muscles

Air Muscles contract by applying compressed air to small rubber tubes encased in a strong plastic netting. There are many benefits to air muscles including their power to weight ratio, lack of stiction and natural damping, all of which make them very suited to applications modelling biological muscles [1]. As with pneumatics, they require a source of compressed air.



Figure 2.3: Air Muscle from the Shadow Robot Group

2.2.2 Muscle Wire

Muscle wires are shape memory alloys, typically an alloy of nickel and titanium. These alloys contract when heated, with control obtained by varying the amount of current, thus heat, passing through the wire. Muscle wires are light and have excellent power to weight ratios, with the ability to lift up to a thousand times their own weight. Whilst individually they do not have much holding force, when grouped together in large numbers similar to a human muscle, they can be quite effective[24].



Figure 2.4: Muscle wire actuated hexapod[20]

2.3 DC Motors

By far the most popular method of actuation in robotics today is the permanent magnet DC motor. Rotary motion is achieved by inducing a magnetic field in a set of windings around a rotor. This magnetic field then seeks to align itself with permanent magnets within the casing of the motor. As the rotor spins, another set of windings is energised, thus causing the rotor to continue spinning. By reversing the voltage applied to the windings, reverse polarity and thus reverse motion is achieved. Current is continuously supplied to the rotor windings by a set of brushes that contact as the rotor spins. Commercial DC motors are generally made for high speed / low torque applications. Several hybrids of DC motors exist, each suited to a different application[10].

2.3.1 Stepper Motors

Stepper motors vary from conventional motors in that the rotor is made up of numerous permanent magnet combinations and the stator holds the windings. Exciting the stator windings causes a magnetic field, which aligns the permanent magnet rotor to the stator. By constantly exciting different pole windings on the stator, it is possible to achieve rotary motion. The output angle of the motor is determined directly from the number of poles and windings, and is quantised, with output angles of 1.8° readily available. More accurate position control is possible through half-stepping, exciting more than one set of stator windings at a time. Stepper motors can be used in an open loop situation, as the output position can be determined by the order and number of windings energised. Despite quite accurate position control being possible, stepper motors have quite low power density and should the motor slip, position can be lost without feedback. Stepper motors can be typically found in computer hard drives and other low torque / high accuracy applications[10].

2.3.2 Servo Motors

Servo motors are simply DC motors with built-in feedback. A potentiometer attached to the output shaft provides position feedback to a controller located in the motor housing. Due to the nature of the potentiometer attached, servo motors typically have a rotation range of less than 320° . Commercial servo motors come complete with gear box and this, all in one package, is highly favoured by hobbyists. The additional circuitry required to support the on board feedback leads to a large case size and diminished power to weight

ratio. Servo motors are however, a cheap and easily interfaced actuator[13].

2.3.3 Linear Actuators

There are two types of Linear Actuators available, electric and mechanical. Electric linear actuators consist of a magnetic carriage moving along an energised track. These are predominantly used in applications such as x-y position tables. Linear actuation is also possible with a mechanical extension of a DC motor. To convert the rotary motion of a DC motor into a linear motion, a threaded rod is attached to the rotor of the motor, along which a lead screw or ball screw device is driven. The main drawback with mechanical linear actuators is that the physical length of the actuator is the length of the greatest extension regardless of the position of the screw or carriage[16].

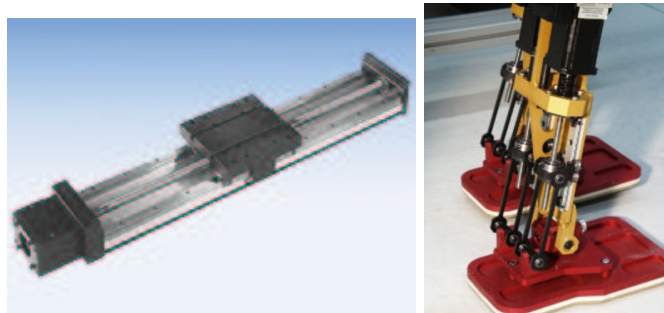


Figure 2.5: (l-r) Linear Positioning System from Lintech[16] and Linear Actuators on INRA's humanoid BIP[4]

2.4 Power transmission

Power transmission devices are generally added onto an actuator to change performance characteristics to suit the individual application. These modifications are typically changes in the torque / speed relationship of the actuator, and a change in the axis along which the power is transmitted.

2.4.1 Pulleys

Power is transmitted in a pulley system by a flexible spline surrounding constant centre separated sprockets. This belt is either smooth (V-belt), or toothed (synchronous timing belt). Smooth belts are cheap but not accurate, as with load they will experience undetermined slip. Synchronous timing belts provide accurate position control, but under high

torque, will suffer the effects of ratcheting, and thus lose their position information. Pulley drive systems have good power transfer ratings as a relatively large amount of belt contact is enjoyed on each sprocket. The torque /speed ratio of a pulley drive system, is simply the ratio of teeth or diameter between the pulley wheels or sprockets involved. As a result of this, ratios larger than 4:1 become unwieldy due to the diameter of the larger sprocket. There are a few drawbacks to pulley drive systems, the efficiency is dependent on the distance between the sprocket centres, and the belts experience some elongation during operation[11].

The torque rating of a drive system is predominantly governed by the rating of the belt. Current belt technology involves the use of polyurethane, with flexible steel cables embedded to provide additional strength. Torque is increased and speed decreased when driving a large sprocket from a small one.[11]

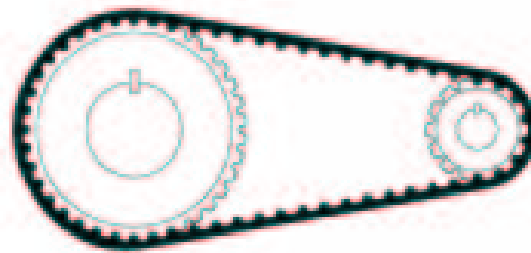


Figure 2.6: Standard Pulley arrangement[11]

2.4.2 Gearhead

As stated above, commercial DC motors are designed for high speed and low torque applications. A gear box can be used to modify the speed and torque ratings to better suit the application. The resulting characteristics of the output shaft are a function of the gear ratio and the efficiency of the gear head. The torque/ speed relationship of the motor shaft to the gear head shaft is as follows:

$$T_{output} = T_{input} \times \eta \times GearRatio$$

$$n_{output} = \frac{n_{input}}{GearRatio}$$

Several types of gear head are available, with reductions up to 1000000 : 1 not uncommon[21].

Spur Gears Spur gears consist of a series of meshing cogs, with one or more sets within the gear head. For each set of cogs, there is an efficiency and ratio that is cumu-

relative to the end of the gear train. Spur gear heads are best suited to low torque applications, as the transmission of power is achieved across only a couple of teeth at a time. Spur gear heads are relatively long and heavy, but quite cheap[21].

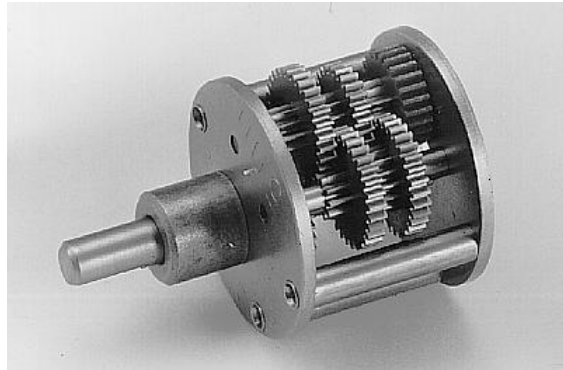


Figure 2.7: Spur Gear cut-away

Planetary Gears Planetary gears are a special type of spur gear. A planetary gear system, has a central sun gear, surrounded by three planet gears, and all encased in an outer spline. As the sun gear rotates, it engages the surrounding planet gears which in turn rotates the outer spline. As the sun gear contacts three gears at any point in time, as opposed to only one with traditional spur gears, a larger amount of torque can be transmitted per stage. Planetary gear heads have a greater gear ratio and torque rating than comparably sized spur gears, but are more expensive[21].

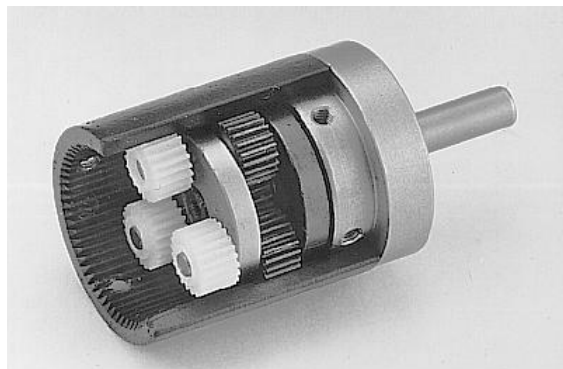


Figure 2.8: 2 Stage Planetary Gear head cut-away

Harmonic Gears Harmonic gearhead are quite new and quite expensive. Harmonic Drive systems consist of a circular spline, a flexible toothed inner spline and an elliptical wave generator. The flexible inner spline has the same pitch diameter as

the circular spline, but has less, typically two, teeth. As the wave generator is rotated, the flexible spline meshes with the circular spline along the major axis of the wave generator. For each complete turn of the wave generator, the flexible spline will counter-rotate by the number of teeth less than the circular spline. As a result of this, quite large reductions can be achieved in a relatively small and light package[12]. Honda employs the harmonic drive system on it's Asimo robot[2].

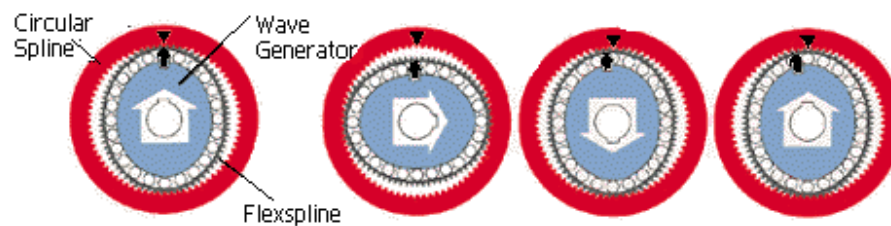


Figure 2.9: Harmonic drive operation[12, modified].

As the elliptical wave generator turns, it engages the flexspline along its major axis. Bearings between the wave generator and the flexspline reduce sliding friction losses. A complete turn of the wave generator results in a 2 tooth retrograde of the flexspline with respect to the circular spline.

2.5 Feedback

Closed loop control is not possible without feedback of some description. By far the most commonly used feedback for revolute joints is the optical encoder. Optical encoders consist of a slotted disk and an infra-red emitter / detector pair, arranged such that rotation of the disk breaks the IR beam of the emitter / detector pair. The frequency and number of pulses generated by this action can be used to obtain position and velocity information. Direction information is also possible with quadrature encoding, which requires another IR pair arranged at a 90° phase shift from the original pair. Encoders with 500 to 1000 counts per revolution are typical[30].

Potentiometers are used less frequently, as they are far less accurate and experience non-linearities close to either limit. Continuous rotation is not possible, and as such are suited to applications requiring at most a few revolutions of the joint. They are however very cheap and are easily incorporated into revolute joints that experience rotation of less than 300° [30].

Chapter 3

Specifications

3.1 The GuRoo

To turn the GuRoo concept into a reality, a set of specifications was devised. The robot was to be human like in appearance, 1.2m tall and approximately 30kg in weight. These parameters were selected to reflect the size of a child of approximately 13 years of age. The GuRoo was also required to be autonomous, so all power and control systems were to be on board[8, 9, 27]. Local vision and internal sensors were to be fed to a central controller, where decisions were made as to the movement of the robot[5, 14, 22, 29]. Velocity commands were then passed along the CAN (Controller Area Network), to a dedicated low level actuator controller[3, 9, 25, 27, 32]. The final application of the GuRoo was to play soccer in a controlled competition.

3.2 Drive System Specifications

3.2.1 Electro-Mechanical Design

Consideration must be given to the physical size and shape of the actuators. They must have an axis of motion easily implemented and must be physically easy to assemble into the robot. Low maintenance and little ancillary equipment required is highly desirable. As the GuRoo is to be totally autonomous, power to weight ratio is important to ensure no 'dead' weight is being carried.

3.2.2 Power

To have a passively stable biped, the robot must be able to hold its whole weight on relatively few joints at some point during its gait. This requires the use of an actuation system that is high in power density but low in weight. The power deliverable by the actuator in both torque / speed and order of magnitude must be sufficient to allow the robot to support its 30kg structure and walk at a speed of 0.1 m/sec. The power consumed is also important, and as the robot is to be autonomous, the power available to the actuators must be sourced from batteries.

3.2.3 Actuator Control

The actuators must be able to be easily controllable. This entails ease of interface with a low level actuator controller board. Appropriate and adequate feedback is necessary to ensure accurate control of the transient response of the actuators. The steady state error is required to be approximately 1mm over the length of the longest possible link.

3.3 Design considerations

3.3.1 Degrees of Freedom

A human has over 200 bones, with 64 in the upper body, 62 in the lower body and the remainder distributed throughout the rest of the body[6]. This large amount of individually controlled links provides countless degrees of freedom. Individual robotic limb projects, such as Utah/MIT's 16 degree of freedom (DOF) dextrous hand[28], have been constructed to closely model the degrees of freedom of real human limbs. Whilst these projects accurately model human degrees of freedom, the technology does not exist to amalgamate these relatively complex limbs into a complete humanoid. As a result of this, a much simplified model of humanoid motion must be used, balancing the capability of the current technology with the reality of human motion. The number and types of degrees of freedom must be selected with this in mind.

3.3.2 Actuator type

Once the degrees of freedom are chosen, the type of actuator required to drive each DOF needs to be decided. Considerations such as power deliverable, as well as package size, weight and shape are all important. The advantages and disadvantages discussed in the

previous chapter must be also considered. Each DOF within the robot must be considered individually and an actuator selected accordingly.

Chapter 4

Initial Humanoid Design

4.1 Humanoid Model

The first stage in modelling a humanoid, is to determine the number and orientation of each degree of freedom. A total of 23 degrees of freedom were chosen, ensuring enough DOF to adequately copy a human, whilst still keeping the required technology relatively simple. These DOF are outlined in Table 4.1 and Figure 4.1. The humanoid is arranged in a star like configuration, with a head, left arm, right arm and waist branching from a torso, and a left leg and right leg branching further from the waist.

Location	No. of DOF ¹	Description
Head	2	Pitch + Yaw
Shoulder	2 x 2	Pitch + Roll
Elbow	2 x 1	Pitch
Waist	3	Pitch + Roll + Yaw
Hip	2 x 3	Pitch + Roll + Yaw
Knee	2 x 1	Pitch
Ankle	2 x 2	Roll + Pitch

Table 4.1: Location and Degrees of Freedom

¹2 x indicates left and right hand side of the humanoid

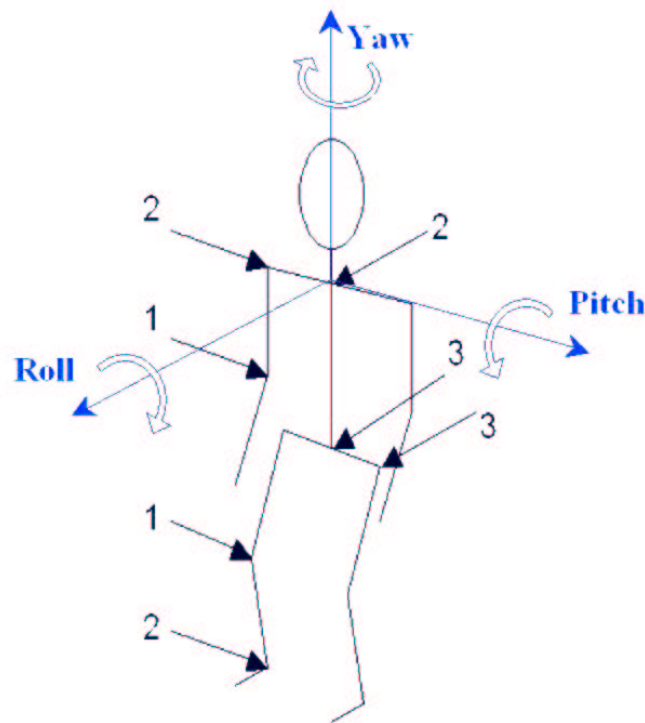


Figure 4.1: Location and Degrees of Freedom Within the GuRoo

4.2 Mechanical Design

Once the location and type of joints was determined, the mechanical design could be undertaken. Solid Edge CAD was used to design the GuRoo, with each part individually modelled in the program. Each link was then assembled from its various parts and the final design a collation of the separate sub-assembly of links. The complete mechanical design process is covered by Wagstaff[29].

4.3 Motor Selection

4.3.1 Upper Body

The upper body consists of 8 degrees of freedom, three for each arm assembly and two for the head and neck. As these joints bear considerably less weight than the lower joints, it was decided to use servo motors for actuation. Servo motors were considered the best alternative due to their low weight and inbuilt control system.

For each of the 8 DoF, the Hitec HS-705MG servo motors were chosen. These motors are the most powerful metal gear, MG, servo motors available with the series chosen ahead

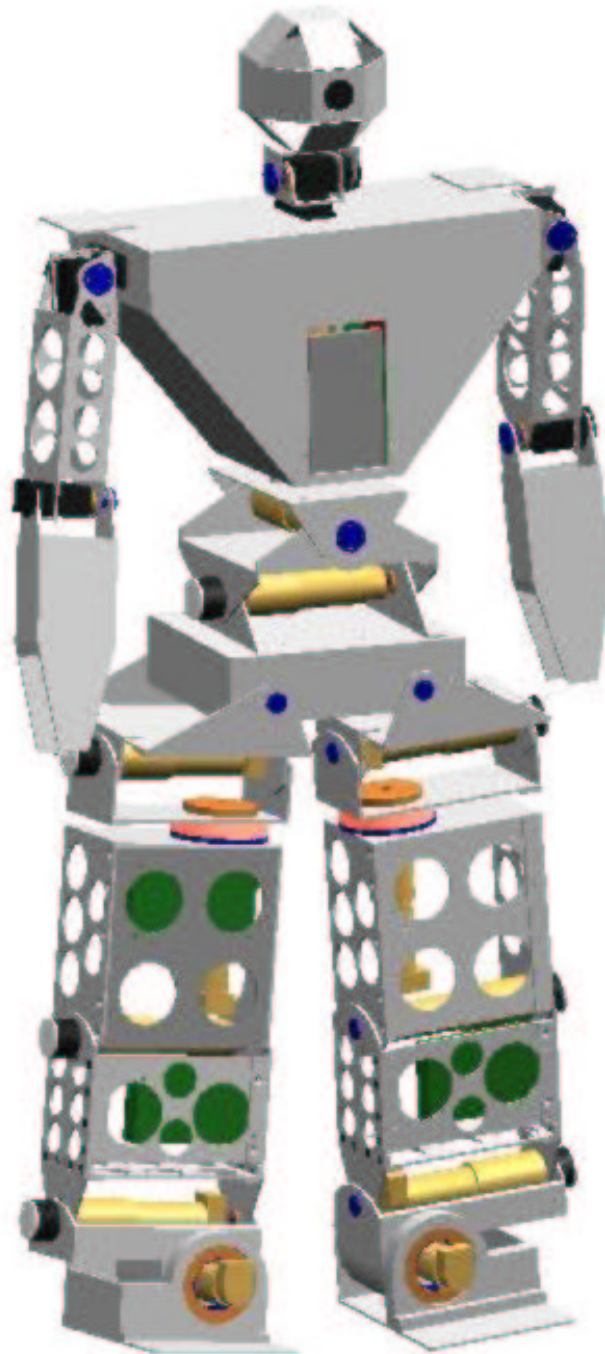


Figure 4.2: Final CAD design

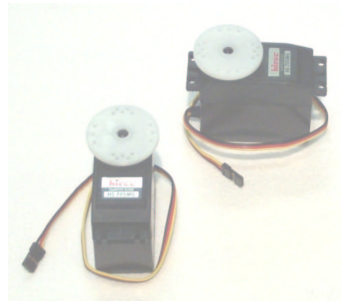


Figure 4.3: Hitec HS-705MG used in the Upper Body

of the nylon gear train series for their strength and durability. They have a maximum output torque of 1.3 Nm. No specifications were available from the manufacturer, and at the time of writing the motors were not yet delivered. As a result of this detailed characteristics of the motors were not available.

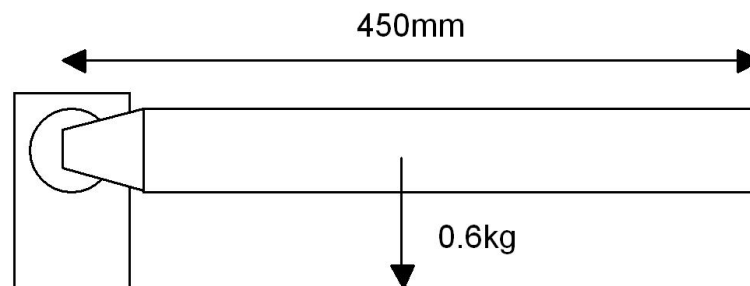


Figure 4.4: Initial Servo calculation.

The worst case scenario for a servo motor occurs at the shoulder when the arm is out at 90° from upright. An initial estimate of 450mm arm length and a maximum torque of 1.3Nm allows the entire arm to weigh no more than 600g.

Using the maximum torque, it is possible to make a rough estimate of the capability of the servo motor. The worst case scenario occurs at the shoulder joint, when the entire arm is out at 90° to the torso. Using an estimated arm length of 450mm, the maximum weight of the arm can be determined by $Mass = \frac{Torque}{distance \times gravity}$. For simplicity the distance at which the mass acts, is half way along the arm. This gives a final permissible mass of the arm of $M = \frac{1.3}{0.225 \times 9.81} \approx 600g$. All 8 servo motors are controlled by a TMS DSP board developed by Cartwright[9].

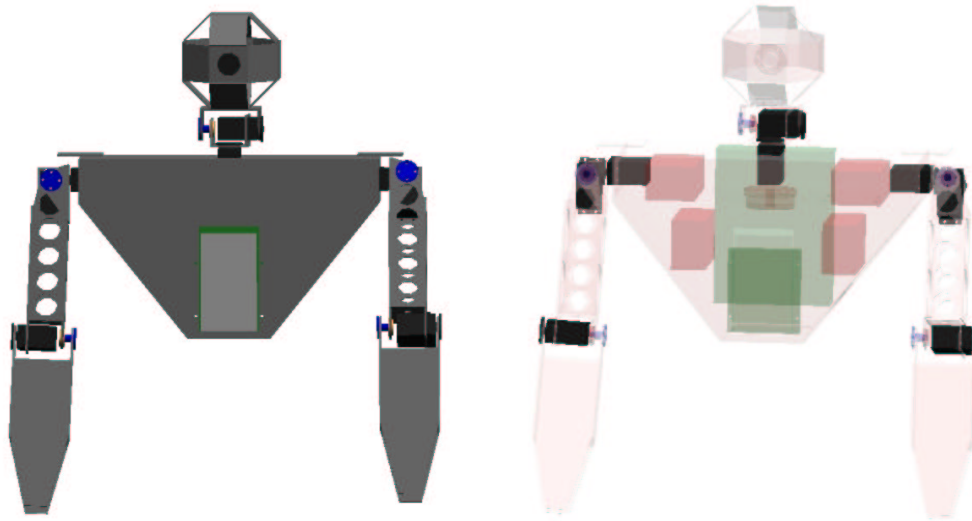


Figure 4.5: Location of Servo Motors

4.3.2 Lower Body

The lower body consists of 15 degrees of freedom, each actuated by a brushed DC motor. In choosing these motors, several factors were considered. They include size, weight, power delivered and cost. The Maxon motor range proved to be the most feasible, as they were in the power range required, and were cheap and readily available. The Modular System employed by maxon, allows a large range of motor, gearhead and encoder combinations[21].



Figure 4.6: Complete Motor / Gearbox / Encoder Combination

Initially, it was thought that a crouching action would be the worst case scenario for the motors. A 30kg robot supported by the knees, with a thigh length of 0.2m, gives a

required torque of $\frac{30 \times 9.81 \times 0.2}{2} \approx 30 \text{ Nm}$ per knee joint. Given a velocity of 2 rad/s, this results in an actuator of the order of magnitude of 60 Watts.

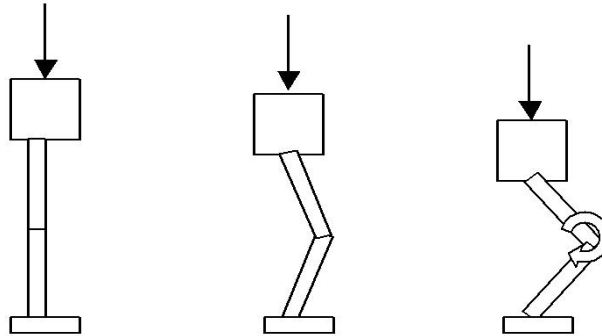


Figure 4.7: Initial Crouching Movement

The initial assumption was made that the knee joints would require the most torque of all the lower limb joints.

There were three motor series that were considered, RE25, RE36 and RE40. The largest gearhead compatible with the RE25 series motor, has a maximum output torque of 4.5 Nm, considerably smaller than that required, and as such were discounted. The relatively high weight of the RE40 series at 480g, relative to the 150W it was capable of generating, was considered unacceptable. Through a process of elimination, the RE36 series was chosen.

The Motor chosen was RE36 70 Watt motor with a GP42 156:1 ceramic gearhead and HEDS optical encoder. Complete Specifications can be found in Appendix E.

Motor	
Nominal Voltage	32V
No Load Speed	6790 rpm
Stall torque	0.832 Nm
Terminal Resistance	1.71 Ω
Torque Constant	44.5 mNm
Rotor Inertia	65.2 gcm^2

Table 4.2: Motor Specifications

A motor control board developed by Stirzaker[27], uses local control by a TMS320F243 Digital Signal Processing Micro-controller and drives three DC brushed motors each with a L6203 motor driver. Each driver, adequately heatsinked, can safely source up to 4A.

From these specifications it is possible to calculate the characteristics of the motor / gearhead / encoder combination.

4.3.3 Gearhead Selection

The GP42 is a multistage ceramic planetary gearhead with ratios ranging from 3.5 : 1 to 936 : 1. The 156 : 1 is the largest ratio available in the 3 stage section, weighing 460g.

The choice of gearhead ratio was made to ensure the maximum output torque, based on a 4A limit from the drivers, was less than the maximum permissible output torque on the gearhead shaft. Should a joint draw more than 4A and hence require over 20Nm of torque, the control system will respond by shutting down power to the appropriate joints.

$$\begin{aligned}
 \text{Maximum Torque} &= k_m \times n_g \times \eta_g \times I \\
 &= 0.0445 \times 156 \times 0.72 \times 4 \\
 &= 19.99 \text{ Nm}
 \end{aligned}$$

Had this 20Nm maximum output torque been insufficient, the next largest gearhead would be a 4 stage planetary, adding an extra 14.5mm to the overall length and weighing an extra 100g.

Using an encoder of 500 counts per revolution through a 156:1 gearhead, a theoretical output precision of $\frac{360^\circ}{500 \times 156} = 4.6 \times 10^{-3}$ degrees per count is possible. Over a typical leg length of 600mm, this gives a linear displacement of $600 \times \tan(4.6 \times 10^{-3}) \approx 0.05\text{mm}$, easily meeting the 1mm limit proposed in specifications.

Gearhead	
Ratio	156:1
Max Efficiency	72%
Max intermitten Torque	22.5 Nm
Max continous Torque	15 Nm
Encoder	
Counts per Revolution	500
Channels	2 + index

Table 4.3: Gearhead / Encoder Specifications

4.3.4 Motor Unit Characteristics

A spreadsheet was used to quickly evaluate the characteristics of a motor combination and is provided in Appendix B. The following is an example of the motor unit's characteristics given operating parameters of 10Nm torque at a speed of 30 rpm.

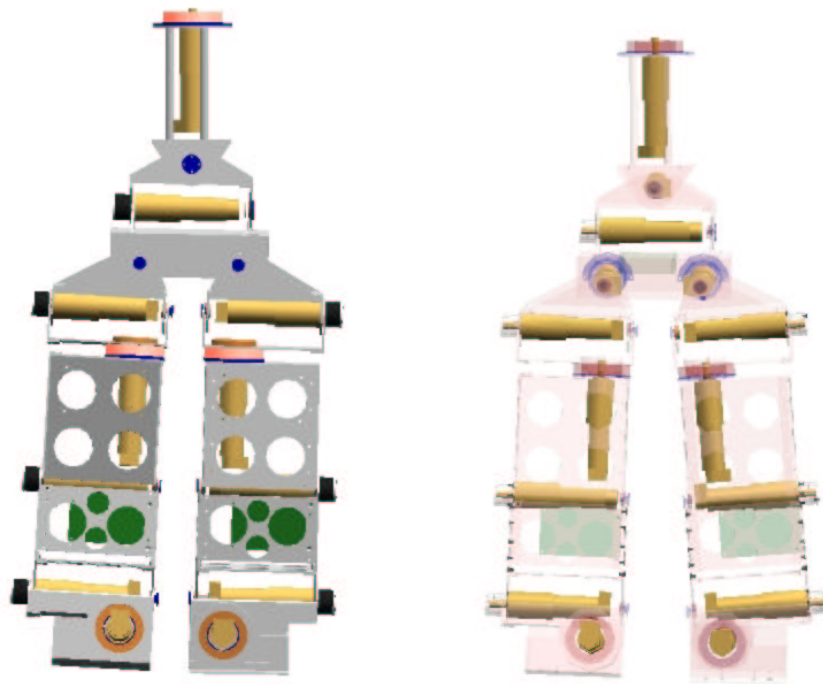


Figure 4.8: Location of the Brushed DC motors in the Lower Body 3 located within the spine, 3 in each hip, 1 in each knee and 2 in each foot.

$$\begin{aligned}
 \text{Torque Constant} &= k_m \times n_g \times \eta_g \\
 &= 0.044 \times 156 \times 0.72 \\
 &\approx 5 \text{ Nm/A}
 \end{aligned}$$

$$\begin{aligned}
 \text{Current drawn} &= \frac{\text{Torque}}{\text{Torque Constant}} \\
 &= \frac{10}{5} \\
 &= 2 \text{ A}
 \end{aligned}$$

From this current it is possible to calculate the temperature rise of the motor.

$$\begin{aligned}
 \text{Temperature} &= (I^2 R \times R_{th}) + R_{ambient} \\
 &= (2^2 \times 1.71 \times 9.8) + 25
 \end{aligned}$$

$$= 92^{\circ}C$$

The R_{th} of $9.8^{\circ}C/W$ is calculated under the test conditions of horizontal mounting on a plastic plate[21]. As in this project each motor is mounted to 3.18mm plate aluminium, R_{th} will be slightly less, giving more favourable temperatures. As can be seen from these calculations, 10Nm at 30rpm is a good operating point in terms of current consumption and power dissipation. Whilst each motor can be briefly overloaded to 20Nm and $125^{\circ}C$, the bulk of any gait should stay around this operating point.

The following calculations are parameters necessary to simulate the motors in the DynaMechs simulation package[18]. All parameters are calculated in SI units.

$$\begin{aligned} \text{Maximum Speed} &= \frac{\text{No Load Speed}}{\text{Gear Ratio}} \\ &= \frac{6790 \text{ rpm}}{156} \times \frac{2 \times \pi}{60} \\ &= 4.56 \text{ rad/s} \end{aligned}$$

$$\begin{aligned} \text{Back EMF} &= \frac{\text{Nominal Voltage}}{\text{No Load Speed}} \\ &= \frac{32}{4.56} \\ &= 7.02 \text{ V/rad/s} \end{aligned}$$

$$\begin{aligned} \text{Output Shaft Inertia} &= \text{Rotor Inertia} \times \text{Gear Ratio}^2 \\ &= 6.52 \times 10^{-6} \times 156^2 \\ &= 0.158 \text{ kgm}^2 \end{aligned}$$

$$\begin{aligned} \text{Coloumb Friction} &= \text{Torque Constant} \times \text{No Load Current} \\ &= 5 \times 0.089 \\ &= 0.445 \text{ Nm} \end{aligned}$$

Viscous Friction Constant:

Maximum Continuous Torque = 15Nm

Maximum Speed = 4.56 rad/s

Motor Power = $15 \times 4.56 = 68.4 \text{ W}$.

The 156:1 gearhead is the largest ratio gearhead in the 3 stage category and as such an efficiency of 70% is assumed based on the maximum efficiency of 72% for all 3 stage gearheads.

$$\begin{aligned}
 P_{lost} &= 68.4 \times (1 - 0.7) \\
 &= 20.52W \\
 &= T_{lost} \times \omega_{nominal} \\
 \Rightarrow T_{lost} &= \frac{20.52}{4.56} \\
 &= 4.5Nm \\
 &= \zeta \times \omega \\
 \Rightarrow \zeta &= \frac{4.5}{4.56} \\
 &= 0.99 \frac{Nm \cdot s}{rad}
 \end{aligned}$$

4.4 Distributed Ball Joint

In each hip joint and the spine, there was required three degrees of freedom. The ideal situation is the ball and socket joint, allowing all three axes of motion to be coincident with a single point.



Figure 4.9: Ball and Socket Joint

An ideal joint allows all three axis of motion to pass through the same pint in space.

The actuation of a ball and socket joint however is quite difficult especially within the space limits imposed to ensure an aesthetic appearance.

The solution devised in collaboration with Wagstaff, was to implement a distributed

ball joint, where each axis of motion within the joint was offset from the previous. By introducing this distribution, it was possible to implement all three axes of motion into a relatively small size.

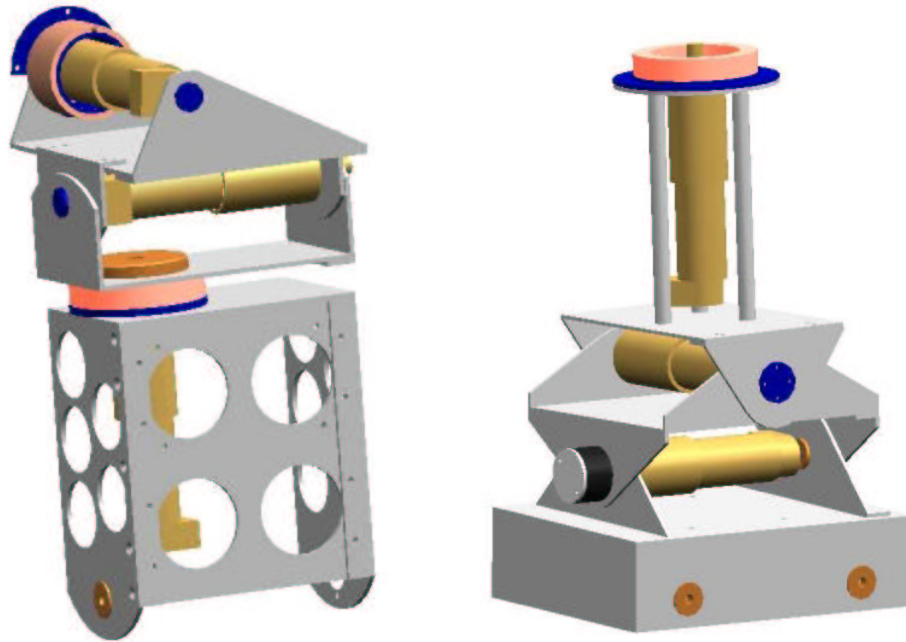


Figure 4.10: (l-r) Distributed Hip and Spine Joints

From the Hip to the Upper Leg, the distributed hip joint axes are Roll, Pitch and finally Yaw. From the Hip link to the Torso, the axes of motion along the spine are Pitch, Roll and Yaw

4.5 Power Transfer

Transfer of the power generated is achieved through a boss and cap assembly placed over the motor shaft. The key in the motor is located with a slot in the boss, and held in place with a grub screw 90° to the axis of motion.

4.6 Pulleys

An initial assumption was made that the joints requiring the most torque would be the Pitch motors in each leg. To obtain additional torque at these joints involved the addition of a 4:1 pulley system. To achieve good efficiency and no ratcheting in a pulley system,



Figure 4.11: Boss and End Cap Assembly with Maxon Motor

there needed to be considerable belt tension between the sprockets. Figure 4.12 shows the setup required for a 4:1 ratio pulley setup[11].

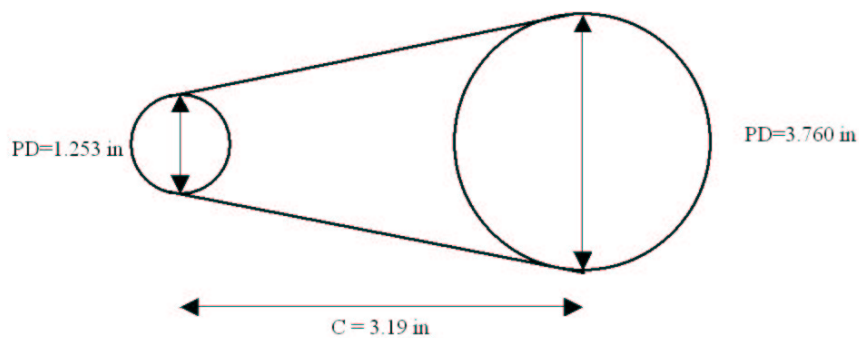


Figure 4.12: Initial Pulley Design

The static installation centre tension of the driven sprocket can be calculated by,

$$T_{st} = \frac{17.4 \times HP}{S} + mS^2$$

where,

HP = Designated Horsepower of the motor

S = $\frac{PD \times RPM}{3820}$

m = 0.26 (Table 3 from [11])

$$\begin{aligned} HP_{motor} &= Motor Power \times 1.34 \times 10^{-3} \\ &= 68.4 \times 1.34 \times 10^{-3} \\ &= 0.092 Hp \end{aligned}$$

$$\begin{aligned} S &= \frac{PD \times RPM}{3820} \\ &= \frac{1.253 \times 43.5}{3820} \\ &= 0.0143 \end{aligned}$$

$$\begin{aligned} \Rightarrow T_{st} &= \frac{17.4 \times 0.092}{0.0143} + 0.26 \times 0.0143^2 \\ &= 111.9 \text{ pounds} \\ &= 497.9 \text{ N} \end{aligned}$$

This force is the installation force required, and will increase while in operation. With a maximum radial shaft load of 150N, it is obvious that the tension needed for efficient operation would snap the output shaft of the motor. Strengthening attachments such as outrigger bearings were considered to support the output shaft. After a re-evaluation of the torques required, based on preliminary results obtained in collaboration with Smith[25], the use of a pulley system was considered unnecessary.

Chapter 5

Actuator Simulation

5.1 Simulator

The simulator is based on the the DynaMechs package constructed by McMillan[18]. This program is a dynamic simulator for multi degree of freedom robots with either a tree or star configuration. By creating an accurate model of the humanoid in the simulator, the various forces experienced and torques required could be calculated. The controller boards and the communication between each was also modelled[25].

5.2 DM file Structure

The simulator requires a humanoid model and this is provided with the .dm file. This file completely describes the humanoid model, from the type and number of joints through to mass distribution and other physical properties. The base link of the GuRoo is its Torso link, which in this application is considered a mobile base link, with 6 degrees of freedom. The complete .dm file can be found in Appendix A.

The following is the .dm code required for a typical link within the model.

```

RevoluteLink {                                #Waist2
  Name "Waist1"
  Graphics_Model "Graphics//waist2.wrl"
  Mass 1.948000
  Inertia 0.028552 -0.000003 0.000095
          -0.000003 0.027092 0.000590
          0.000095 0.000590 0.003277
  Center_of_Gravity -0.000240 -0.001316 0.090517
  Number_of_Contact_Points 4
  Contact_Locations 0.097 -0.05 -0.05
                   0.097 -0.05 0.05
                   0.097 0.05 -0.05
                   0.097 0.05 0.05
  MDH_Parameters 0 1.57 0.067 0.00
  Initial_Joint_Velocity 0.0
  Joint_Limits -3.1416 3.1416
  Joint_Limit_Spring_Constant 50.0
  Joint_Limit_Damper_Constant 5.0
  Actuator_Type 0
}

```

A brief description of the minor characteristics follows with the more important parameters described in more detail in later sections of the chapter.

Graphics_Model The .wrl graphics file used by the simulator. This graphics model has no effect on the dynamics of the robot.

Mass The mass of the complete link

Centre_of_Gravity The location of the centre of gravity with respect to the co-ordinate frame

Contact_Locations This is based on the Number_of_Contact_Points parameter, and describes the location of key physical points of the link. The simulator uses these points to determine if a link come into contact with another link or the ground. Should a ‘clash’ of links occur, an error is generated in the simulator. The most important set of contact points are those found in the feet, as they describe the contact of the foot with the ground.

Initial_Joint_Velocity As the name implies, each link can be given an initial velocity.

Joint_Limits For each joint, positional limits are specified. Should the joint try to exceed these limits, the joint will act as a damped spring as defined by the Joint_Limit_Spring_Constant and Joint_Limit_Damper_Constant parameters.

5.3 mDH parameters

For each joint along a branch, a co-ordinate frame is assigned. By assigning these frames according to the modified Denavit-Hartenberg (mDH) rules, major computational saving is achieved when evaluating the forward and inverse kinematic properties. The mDH constants consist of four unique parameters that describe the coordinates of the next joint in terms of rotation and translation from the coordinate frame of the preceding joint. Unlike traditional DH parameters, where the displacement is calculated from the joint directly following the base link, mDH parameters are calculated from the base link itself[31].

Revolute actuators are used for each joint in the humanoid and as such the z axis of each lies along the axis of motion of the joint. The x axis of the following link is assigned such that it is parallel to the common normal of the axis of motion of the two joints. The y axis is then calculated using the right hand rule. The sign convention for rotation was chosen such that natural movement away from a set standing position is considered positive[31].

Once these Coordinate frames are determined, the four mDH parameters can be calculated[31].

θ_i is the angle from the x_{i-1} axis to the x_i axis measured about the z_{i-1} axis. For all revolute joints this represents the variable angle of the joint.

d_i is the distance from the x_{i-1} axis to x_i axis measured along the z_{i-1} axis.

l_i is the distance from the z_{i-1} axis to the z_i axis. It is also know as the common normal distance. The length of each link is either an l or d parameter.

α_i is the angle between the z_{i-1} axis to the z_i axis measured about the x_i axis using the right hand rule.

5.4 Coordinate Frames

Once the coordinate frames are established, graphics files are created from SolidEdge for use in the simulator. Each solid model is imported to SolidWorks and a .wrl file generated. While it is possible to generate a .wrl file for the designed link, the large number of surfaces inherent in the complex design can drastically slow the simulator. Instead, a simplified model of the same basic shape and proportion of the original link is used.

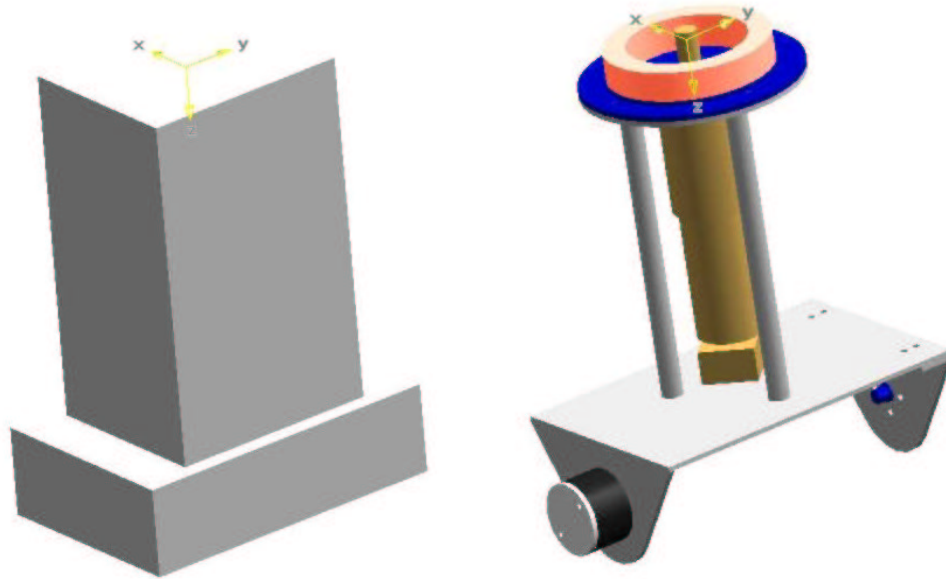


Figure 5.1: Upper Leg Coordinate frame

The simplified block model has less surfaces than the actual CAD link, which greatly reduces the simulation time to real time ratio.

5.5 Inertia Tensors

The inertia tensor and centre of gravity for each link is calculated with respect to its coordinate frame. The inertia tensor of a rigid body is the tensor necessary such that the product of the angular velocity with the inertia tensor will give the angular momentum of the rigid body. It takes the form of

$$I = \begin{pmatrix} I_{xx} & -I_{xy} & -I_{xz} \\ -I_{yx} & I_{yy} & -I_{yz} \\ -I_{zx} & -I_{zy} & I_{zz} \end{pmatrix}$$

where I_{xx} , I_{yy} and I_{zz} are the moments of inertia around the coordinate axis and the remaining terms are known as the products of inertia. The inertia tensor is symmetrical and as such $I_{xy} = I_{yx}$ and so on for all other products of inertia[15].

Solid Edge can calculate many physical properties of an assembled link. From the file generated, the important parameters of mass, centre of gravity and the inertia tensor are extracted. Superfluous information, such as principle axes and centre of volume provided by SolidEdge were not required.

The first revision of the humanoid .dm file was built with the inertia tensor of each link modelled as a cylinder. Subsequent revisions of the mechanical design led to quite

complex links, consisting of the main aluminium structure right down to the bearings and screws.

5.6 Z screw Link

The z screw link is used to implement a constant z axial screw transformation for a coordinate frame. This link type has no physical properties and as such does not have an impact on the dynamics of the model. The axial screw transformation is implemented as a constant angular and linear displacement along the z axis of the preceding joint coordinate frame. This relates to a d_i and θ_i component in mDH terms[18, 19].

5.7 Actuator Types

There are two distinct actuator types available in the DynaMechs simulation package. Type 0, is a generic revolute link, with only a joint friction parameter associated. As such it is treated as an ideal motor with infinite torque and speed. This actuator is used to model the servo motor as insufficient specifications were available. Actuator type 1 is currently the only other actuator type available and models a revolute brushed DC motor. The following parameters are added to the .dm file when using actuator type 1[19].

```
Actuator_Type 1
Motor_Torque_Constant 5
Motor_BackEMF_Constant 7.02
Motor_Armature_Resistance 1.71
Motor_Inertia .111
Motor_Coulomb_Friction_Constant 0.445
Motor_Viscous_Friction_Constant 1.15
Motor_Max_Brush_Drop 0
Motor_Half_Drop_Value 1
```

The maximum motor drop and half drop values are parameters associated with much larger motors, and relate to the characteristics of the commutative brushes within the motor. As considerably smaller motors were used in this application this led to the default values being used. The results shown above have been calculated in the previous chapter. It must be remembered that when the simulator requests motor specifications, it is referring to the motor / gearhead combination, not the motor itself. Using this actuator type, it was possible to implement current and torque limits for the motor thus more accurately modelling the humanoid.

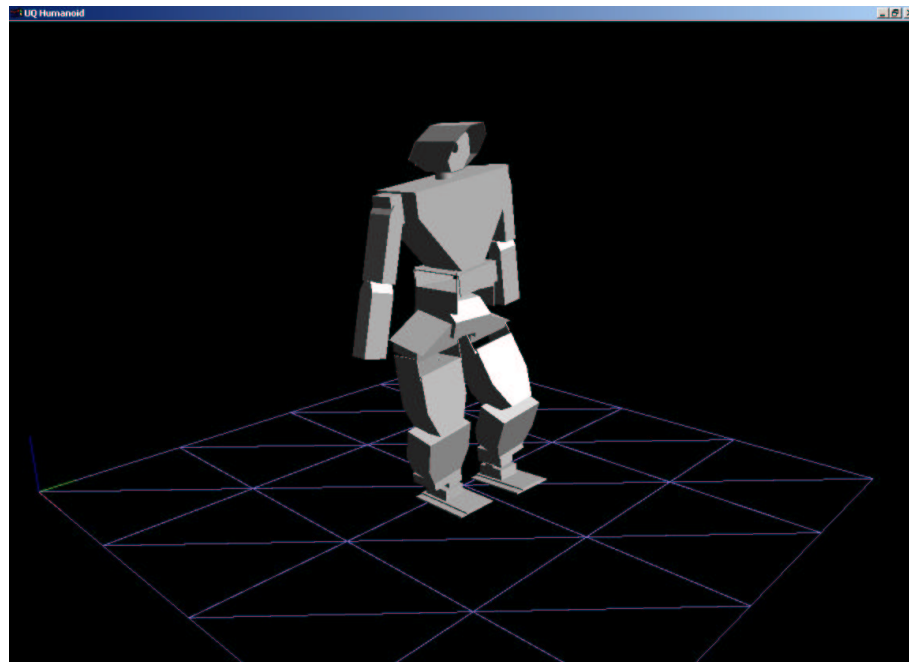


Figure 5.2: Current Simulator Graphics Model

Chapter 6

Simulation Results

Two initial movements were applied to the humanoid to evaluate the suitability of the motors chosen. They were a crouching movement and lifting one leg. Data is logged from the simulator recording positional error, torques, currents, velocity etc. at 5 ms intervals. A Matlab script was used to graph the information in the log file.

6.1 Crouching

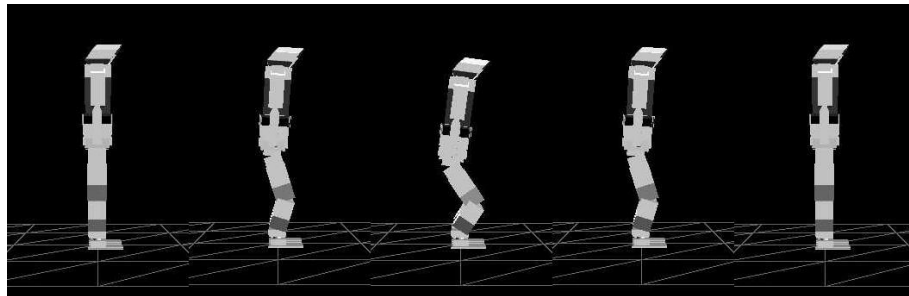


Figure 6.1: Crouch Simulation

The first action simulated was a crouching motion. As the feet never leave the ground with this movement, it is very stable and easily implemented. The graphs in Figure 6.2 show the torque on each Pitch motor in each leg. Both the left and right graphs have the same shape and order of magnitude as expected from a symmetrical crouch movement. The slight differences are a result of the minor differences when evaluating the inertia tensor of each link. The left leg appears to take slightly more weight as shown by the marginally higher torques.

Hip Pitch	30°	Down Time	2 sec
Knee Pitch	50°	Hold Time	1 sec
Ankle Pitch	25°	Up Time	1 sec

Table 6.1: Crouch Parameters

As can be seen from the Figure 6.2, all motors exert a positive torque in the initial stages of the movement. This is expected as the quite large mass of the robot must accelerate from a stationary start resulting in an error between the actual position and the desired position. Each motor is controlled by a PD controller[32] and as the positional error increases, the motor exerts more torque in an attempt to decrease this error.

As each joint gets closer to its desired position, it reverses direction, and falls to a constant holding torque. This torque for each motor is within the recommended operating point of the motor, although the knee motors at, 18Nm holding torque, cannot remain in this position long as they exceed the maximum continuous torque of the gearhead.

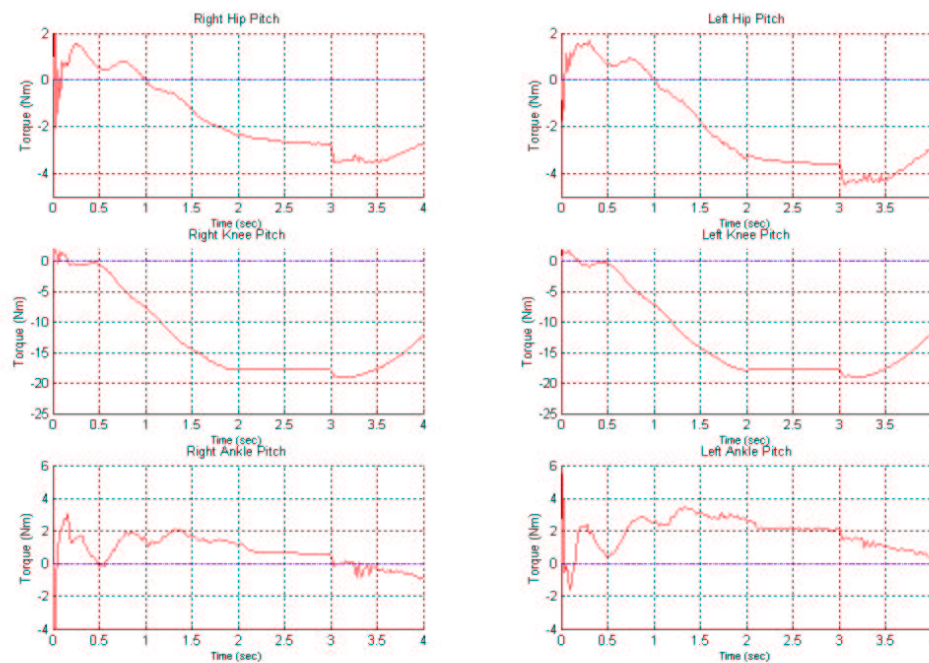


Figure 6.2: Motor Torques for initial Crouch movement

The Knee motors fail just after the 3 second mark, as the torques exceed the maximum intermittent output torque of the gearhead.

The problem arises as the robot tries to stand back upright. Each motor must accelerate the robot's mass against gravity back into an upright position. Both the hip and ankle motors are able to easily cope with this movement, staying well within the peak limit of 22Nm. The knee motors however would fail as they exceed this maximum intermittent torque rating. The 0.5 Nm step on all graphs at the 3 second mark is a result of the stiction in the motor model that needs to be overcome from any standing start.

The failure of these motors then begs the question, 'What can be done to ensure motors do not fail?' There are several options that can be considered, reducing weight, changing motors or modifying the gait parameters. Considerable reduction of weight was not feasible, as the actuators comprise a large portion of the weight, and the vast majority of the aluminium structure has already been milled out to reduce weight. Different motors were also not a possibility, as the failing factor of the crouch was the torque on the gear shaft exceeding specifications. The next largest rated gearhead is the GP62, and whilst it has a rated torque of up to 50Nm cyclic, it is not directly compatible with the RE36 series motor and weighs 1.25kg, 790g more than the GP42.

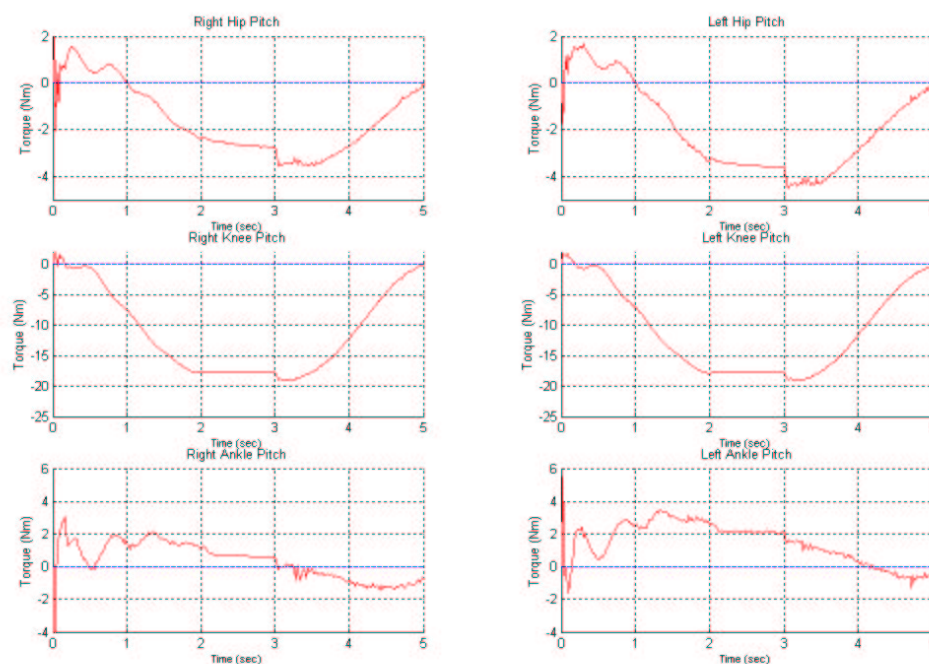


Figure 6.3: Motor Torques for modified crouch

The longer rise time allows the knee motors to stay within maximum rated limits of the gearhead

The only feasible solution is to change the gait parameters. All motors are well within operating limits when the robot is stationary, which implies through careful motion planning the problem of exceeding maximum torques can be overcome. As the torque surges are due to the large positional error, reduction of this error will naturally keep the motor within limits. This can be achieved in this case by extending the 'up time' of the movement. Figure 6.3 shows the motor torques for the same movement amended for a 2 second rise time as opposed to the previous 1 second. The knee joint now stays within the maximum intermittent output torque. This proves that through careful analysis of joint trajectory, similar problems can be overcome.

The longer rise time over 2 seconds eases the load on the knee motor, and brings all motor torques back to acceptable limits. From these results it is apparent that the motors can handle a crouching movement. But this is still far from a complete justification of the motor selection. The next experiment performed simulated the robot standing on one leg.

6.2 Standing on One Leg

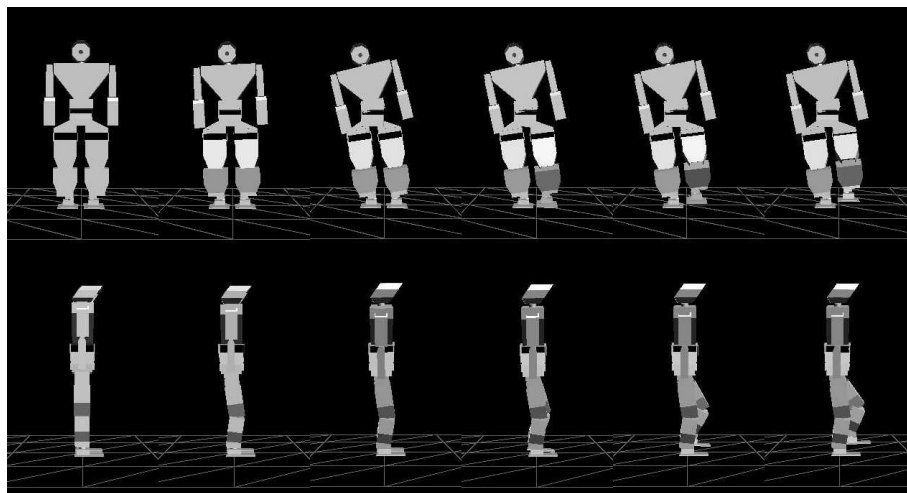


Figure 6.4: Standing on One Leg Simulation

The Standing on One Leg movement can be broken down into a series of joint movements over a five second period. Table 6.2 and Figure 6.5 outline the time taken and angle each joint moves through.

As with the crouching movement, torque / time curves for each joint was logged and graphed. All graphs can be found in Appendix C. Figure 6.6 shows a selection of the most important joints in the movement.

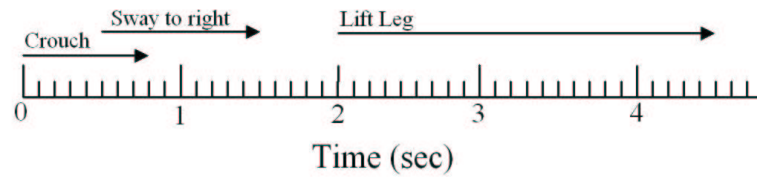


Figure 6.5: Time line of Standing on One Leg Movement

Crouch	Angle	Time Frame
Hip Pitch	12°	0 → 0.8 sec
Knee Pitch	18°	
Ankle Pitch	10°	
Sway to Right		
Hip Roll	5°	0.5 → 1.5 sec
Ankle Roll	5°	
Lift Left Leg		
Left Hip Pitch	17°	2 → 4.5 sec
Left Knee Pitch	25°	
Left Ankle Pitch	10°	

Table 6.2: Standing on One Leg joint times and angles

Both the Right Hip Pitch and Right Knee Pitch joints require a surge in torque just after the 2 second point in the simulation. This occurs as the left leg is lifted at the 2 second mark, and the right leg must bear the entire weight of the robot. The Left Hip Pitch joint also experiences quite a large torque as it lifts and then holds the leg up. The jittering of the torques in the graphs are a result of the links oscillating and can be minimised by careful selection of the PD parameters within the control loops.

The Right Hip Roll motor though will fail as soon as the leg is lifted. This is understandable as the centre of gravity of the robot is supported quite a distance to the left of the Roll joint. This torque can be reduced by swinging the torso to the right in an attempt to counter balance the robot, but the effect while beneficial, is not sufficient to bring the motor within its operating limits. The fact that the Hip Roll motor fails, counters the previous assumption that the Pitch joints would experience the greatest torque.

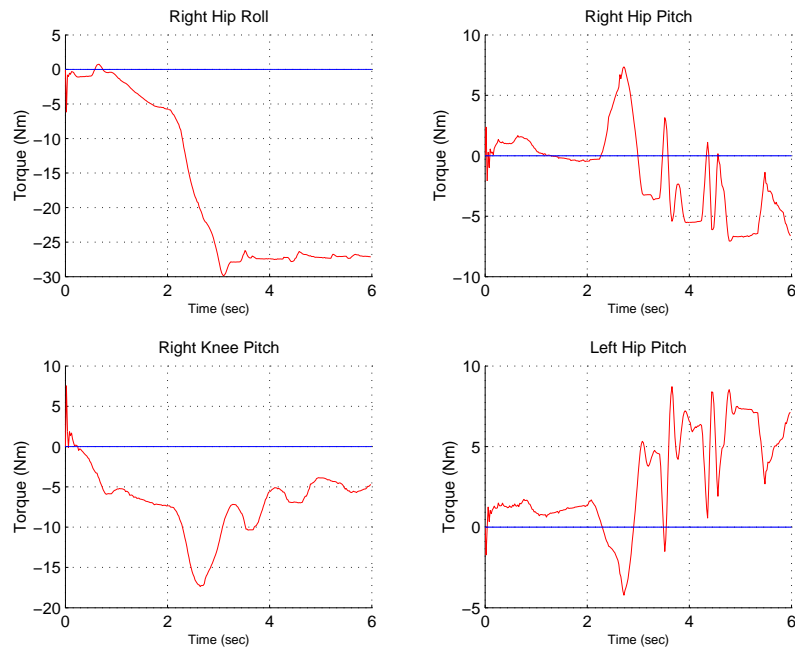


Figure 6.6: Selected Motor Torques for Standing on One Leg movement

6.3 Spring Implementation

A change of actuator was unfeasible, as was pointed out in the previous section, so some method of ‘helping’ the two Hip Roll motors was needed. It was decided that a torsional spring, acting along the same axis as the motor, would be able to store energy, for use when the motor required it.

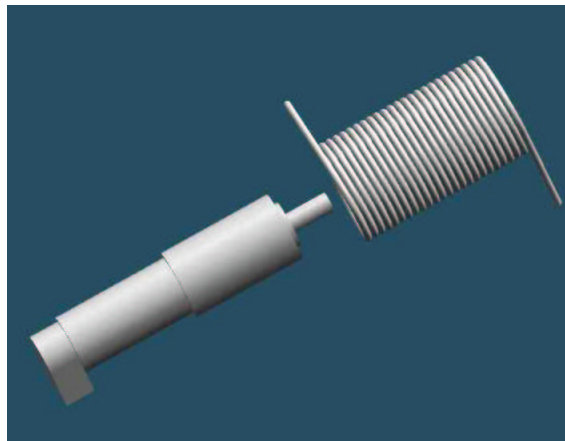


Figure 6.7: Spring / Motor combination

By placing the neutral position of the spring so that it aligns with the neutral position of the legs, any sway away from the centre will result in the energy stored in the

spring from the angular compression, contributing a torque proportional to the the angular displacement. If the neutral position of the spring is located such that the legs are ‘sprung’ out, greater contributed torque is possible. This contributed torque is adjustable, proportionally dependent on the angle that the legs are initially sprung.

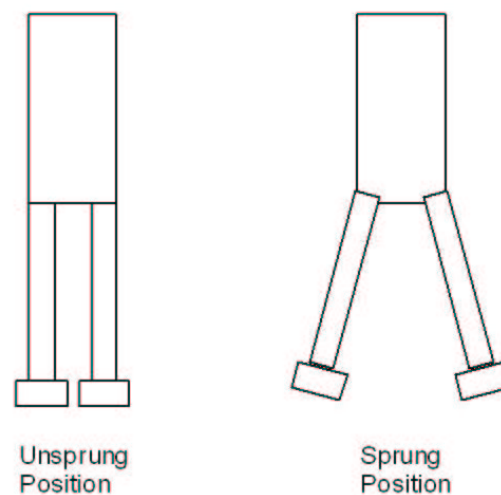


Figure 6.8: Spring Implementation

The movement of each leg against the sprung position, stores energy in each Hip Roll joint. This results in a contributed torque proportional to the angular displacement of the spring.

Currently the movement requires a 5° sway to the right. Coupling this with an initial springing of the legs out to 10° , gives a final contribution of 15° of angular displacement. A torsional spring with a spring constant of 1 Nm / degree , will contribute approximately 15 Nm to each Roll joint. This will then bring the torque required by the Roll motor down to an acceptable 10 Nm .

6.4 Modelling the Spring

A spring can be modelled in the .dm file by constraining the joint limits and setting a value for the Joint_Limit_Spring_Constant. An assumption was made that the spring constant parameter would have the SI units of Nm/rad . A spring of 1 Nm/degree , implied a spring constant value of 57.3 Nm / rad . A single degree of freedom .dm model was created in which to test the spring implementation.

This model consisted of a point mass located along a 1 m link from the base. The point mass was given a negligible weight to negate the effect of gravity and was initially sprung

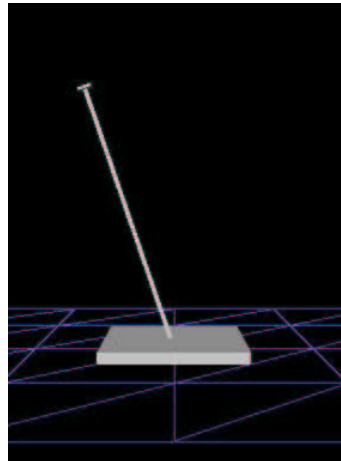


Figure 6.9: One Degree of Freedom simulator model

5° from an upright centre position. The movement consisted of holding the link vertical for 2 seconds before moving to the initial position and another 5° further. The results indicated however an 8 Nm torque required to hold the link upright, and a further 8Nm to hold it 5° below the initial position.

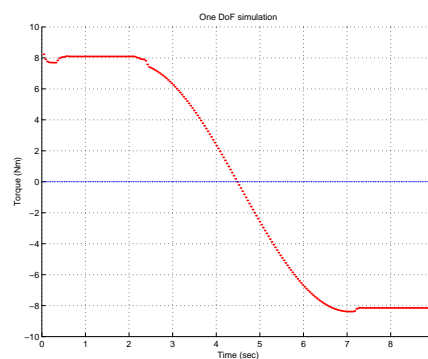


Figure 6.10: Spring Torque based on theoretical spring constant
The calculated spring constant of 57.3 Nm/rad gave a holding torque of 8Nm at 5° , instead of the 5Nm that was expected.

Through trial and error, the spring constant to use was found to be 33.105, although how this relates to the .dm file is still unknown. Two movements were tested, one at 5° and one at 10° , with the results displayed in Figure 6.11.

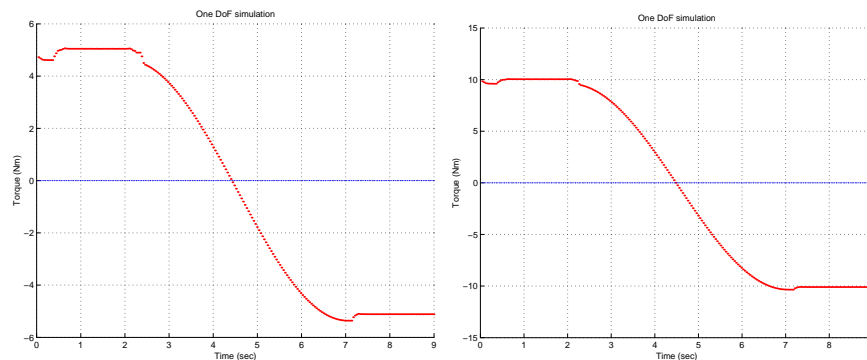


Figure 6.11: Spring Torque based on estimated spring constant
 (l-r) Using a spring constant of 33.105 Nm/rad, a test of the 1 DoF system sprung at 5° and 10° gave holding torques of 5 and 10Nm respectively.

6.5 Spring Implementation

This spring model was then incorporated into the humanoid .dm file by changing the Joint_Limit and Joint_Limit_Spring_Constant parameters. A value of -0.1745 radians for both the positive and negative rotation of both Left and Right Hip Roll was used. The same sequence of movements applied in Section 6.2, were again applied, the results logged and a selection of joint torques plotted in Figure 6.12. The complete set of graphs for this movement can be found in Appendix C.

Both the Hip Pitch graphs and the Right Knee Pitch graph are similar to the unsprung humanoid, with the greatest difference evident in the Right Hip Roll motor as was expected. With a limit of 6 Nm, this motor quite easily fell within operating limits of the DC motor.

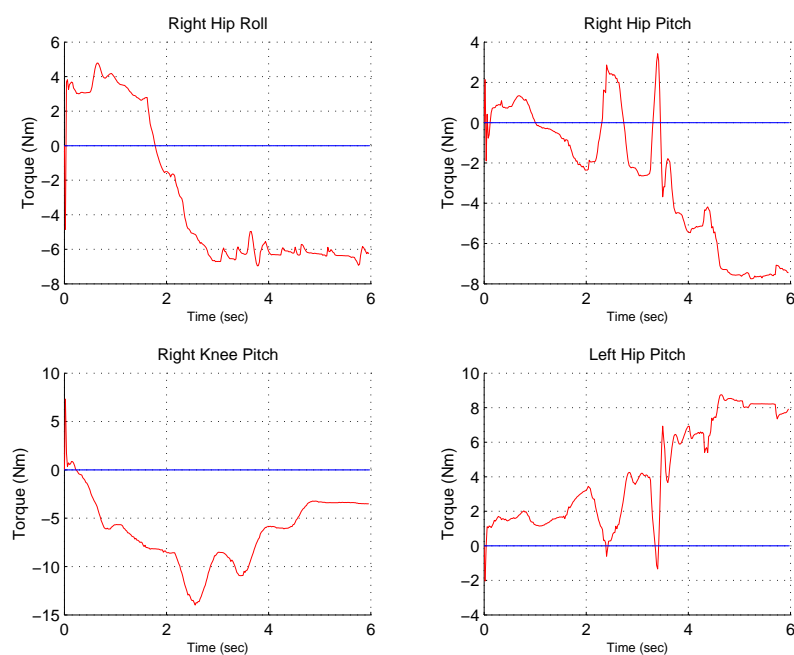


Figure 6.12: Selected Motor Torques with Spring Implementation
The Right Hip Roll motor has been reduced from approximately 25Nm to 7Nm with the implementation of the spring.

Chapter 7

Conclusion

Unfortunately, due to time restrictions, the GuRoo was not built and consequently did not play soccer, as had originally been hoped. Construction had begun with several links complete. By the end of the year, a set of legs will hopefully be completed. The simulator however provides proof of concept, with the action of supporting the entire weight on one leg and demonstrates that the actuators chosen could cope with possibly the worst case scenario for a humanoid robot. The construction of a complete walking cycle was developed by Smith [25] using the humanoid model described above. Smith was able to make the robot walk statically, at a speed of 0.3m/sec, with all DC motors staying within operating limits. These results validate the choice of motors for the GuRoo.

The introduction of a spring in the two Hip Roll motors provides a pronounced and easily implemented benefit, which leads to the possibility of springs in other joints. As with the hip roll joints, gravity can be used to help store energy in the spring until the need arises in which the joint motor must move the associated link against gravity.

7.1 Further Work

Despite achieving the intended goal initially set out in this thesis, there is substantial further work to be done with actuator selection. The actuators that were selected fulfill all the requirements of basic static walking. There are a multitude of other tasks that will no doubt be introduced in the near future. They include

- Standing up from a lying position
- Carrying objects in its hands

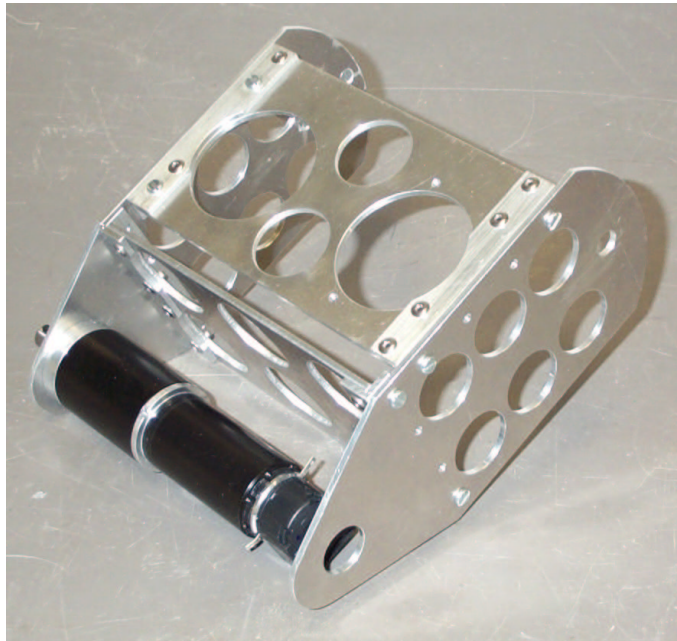


Figure 7.1: Lower Leg link in progress.
The motor at the driven end and the boss at the lazy end have been assembled.

- Running
- Jumping
- Falling without damaging itself

The actuators currently chosen would have difficulty meeting all these quite involved movements for a few reasons. The majority of the DC motors in the lower body are currently pushing their operating limits, and should an unexpected situation occur, such as falling over, there exists a real possibility of serious damage.

The servo motors in the upper body are weak in comparison to the DC motors, and as such, the arms are quite light. A human uses it's arms to shift its centre of gravity when walking, but because of the humanoid's lightweight arms, they do not contribute much to the overall centre of gravity. In fact Smith does not swing the arms at all in his walking gait. More powerful upper body motors however presents the problem of adding significantly extra weight to the robot. The arms currently have no useful hands and the implementation of anything from a 1 degree of freedom gripper through to a fully actuated, 5 fingered hand is possible.

The ideal actuator combination would be a powerful pancake motor coupled with an harmonic gearhead. This would result in much reduced weight and length. The harmonic

gearhead would be able to supply the required torque in a package much smaller than a standard planetary or spur gearhead, as would a high quality pancake motor. The current length of the DC motors defines the leg width, with the considerable saving in length afforded by the pancake / harmonic option resulting in a lighter mechanical structure.

With the delivery of the servo motors, characteristics such as current draw can be measured. A motor model based on Actuator Type 1, can then be constructed and implemented in the humanoid .dm file. The other major improvement to be made to the .dm file is the accurate modelling of contact points. At the moment, no real interest is paid to collision of links and as such possibly illegal joint trajectories are being performed.

Bibliography

- [1] Air Muscles: ShadowRobot Group. www.shadow.org.uk/products/airmuscles.shtml , December 1999
- [2] Asimo: Honda Motor Company. <http://world.honda.com/ASIMO> , Current October 2001
- [3] Bebel B. *Design and Implementation of USB to CAN bridge for the GuRoo Project*. University of Queensland, 2001
- [4] BIP2000 Anthropomorphic Biped Robot. <http://www.inrialpes.fr/bip> , Current August 2000
- [5] Blower A. *Vision System for a Humanoid*. University of Queensland, 2001
- [6] Bones and Muscles: ScienceNet. http://www.sciencenet.org.uk/database/Biology/Bones_and_Skeletons/b00219b.html , Current October 2001
- [7] Brain M. *How Hydraulic Machines Work*. <http://www.howstuffworks.com/hydraulic1.htm> , How Stuff Works. Current October 2001
- [8] Brewer N. *Power System for a Humanoid*. University of Queensland, 2001
- [9] Cartwright T. *Design and Implementation of Small Scale Joint Controllers for a Humanoid Robot*. University of Queensland, 2001
- [10] Fraser C., Milne J, *Electro-Mechanical Engineering*. IEEE Press, 1994
- [11] Gates Rubber Company, *PowerGrip GT2 Belt Drive Design Manual*. <http://www.gates.com/catalogs/index> , March 2000
- [12] Gear Concept. Harmonic Drive. http://www.harmonicdrive.de/2_2_e/e2_2_2.htm , Current October 2001

- [13] Hitec RCD HS-705MG Servo Motor. <http://www.hitecrcd.com/Catalog/Servos/HS-705.htm> , Current October 2001
- [14] Hosking S. *High Speed Peripheral Interface*. University of Queensland, 2001
- [15] Inertia Tensor. <http://kwon3d.com/theory/moi/iten.html> , Current October 2001
- [16] LinTech. *Positioning Systems Catalogue*. 2000
- [17] LynxMotion Inc. <http://www.lynxmotion.com> , Current October 2001
- [18] McMillian S. *Computational Dynamics for Robotic Systems on land and Under Water*, Ohio State University, 1994
- [19] McMillian S. *DynaMechs Simulation Library*. http://dynamechs.sourceforge.net/ref_manual.ps , Current October 2001
- [20] Matthews J. *Stiquito. Muscle Wired Hexapod*. <http://www.generation5.org/stiquito.shtml> , April 2001
- [21] Maxon Motors. ftp://ftp.maxonmotor.com/Public/Download/catalog_2001/Pdf/01_Explanation_DC_49_e.pdf , Current October 2001
- [22] Prasser D. *Vision system for a Humanoid*. University of Queensland, 2001
- [23] Robocup Official Webpage. <http://www.robocup.org> , Current October 2001
- [24] Robotbooks http://www.robotbooks.com/Muscle_Wires.htm , Current October 2001
- [25] Smith A. *Simulator Development and Gait Pattern Creation for a Humanoid Robot*. University of Queensland, 2001
- [26] Sony SDR-3X. <http://www.sony.co.jp/en/SonyInfo/News/Press/200011/00-057E2> , November 2000
- [27] Stirzaker J. *Design of DC Motor Controllers for a Humanoid Robot*. University of Queensland, 2001
- [28] UTAH/MIT Dextrous Hand. <http://www-robotics.cs.umass.edu/p50/utah-mit-hand.html> , August 1994

-
- [29] Wagstaff M. *Mechanical Design for a Humanoid*. University of Queensland, 2001
- [30] Wyeth G. *3E281: Robotics Module 1, Robotic Hardware* http://www.itee.uq.edu.au/~elec3700/ELEC3700_M1.pdf , Current October 2001
- [31] Wyeth G. *3E281: Robotics Module 5, Robot Arms*. http://www.itee.uq.edu.au/~elec3700/ELEC3700_M5.pdf , Current October 2001
- [32] Zelniker E. *Joint Control for an Autonomous Humanoid Robot*. University of Queensland, 2001

Appendix A

Humanoid .dm file

```
# DynaMechs V 3.0 ascii
# Humanoid parameter file
# Humanoid dm file
# Revision 5
# 8/7/01
# Damien Kee

Articulation {
  Name "Humanoid"
  Graphics_Model ""
  Position 0.0 0.0 0.0
  Orientation_Quat 0.0 0.0 0.0 0.0

  MobileBaseLink {
    Name "torso"
    Graphics_Model "Graphics//torso.wrl"
    Mass 8.545000
    Inertia 0.131007 0.000206 -0.009948
            0.000206 0.137529 0.000017
            -0.009948 0.000017 0.241439
    Center_of_Gravity 0.108775 -0.000218 0.009615
    Number_of_Contact_Points 8
    Contact_Locations 0.097 0.2 0.02
                    0.0 0.2 -0.02
                    0.097 0.2 -0.02
                    0.0 0.2 0.02
                    0.097 -0.2 0.02
                    0.0 -0.2 -0.02
                    0.097 -0.2 -0.02
                    0.0 -0.2 0.02
    Position 1.0 1.0 1.045
    Orientation_Quat 0.707 0.0 -0.707 0.0
    Velocity 0.0 0.0 0.0 0.0 0.0 0.0
  }

  Branch {
    ZScrewTxLink { #Neck screw 1
      Name "neck_screw_link"
      ZScrew_Parameters 0.0 1.57
    }

    RevoluteLink { #Neck 2
      Name "Neck"
      Graphics_Model "Graphics//zrot20.wrl"
      Mass 0.047
      Inertia 0.000213 0.0 0.0
              0.0 0.00851 0.0
              0.0 0.0 0.00851
      Center_of_Gravity 0.0 0.0 0.0
      Number_of_Contact_Points 4
      Contact_Locations 0.02 -0.025 -0.025
                      0.02 -0.025 0.025
                      0.02 0.025 -0.025
                      0.02 0.025 0.025
      MDH_Parameters 0.0 1.57 0.0 0
      Initial_Joint_Velocity 0.0
      Joint_Limits -3.1416 3.1416
      Joint_Limit_Spring_Constant 50.0
      Joint_Limit_Damper_Constant 5.0
      Actuator_Type 0
    }
  }
}
```

```

    Joint_Friction    0.35
}
ZScrewTxLink {
    Name "neck_screw_link"
    ZScrew_Parameters -0.021 1.57
}
}
RevoluteLink {
    Name "Head"
    Graphics_Model "Graphics//crap_head.wrl"
    Mass 0.516000
    Inertia    0.002546 0.000996 -0.000003
              0.000996 0.004268 0.000001
              -0.000003 0.000001 0.004916
    Center_of_Gravity -0.068962 0.015631 -0.000082
    Number_of_Contact_Points 4
    Contact_Locations    0.04 -0.04 -0.04
                       0.04 -0.04 0.04
                       0.04 0.04 -0.04
                       0.04 0.04 0.04
    MDH_Parameters    0.0 1.57 0.0 1.57
    Initial_Joint_Velocity 0.0
    Joint_Limits    -3.1416 1.57
    Joint_Limit_Spring_Constant 50.0
    Joint_Limit_Damper_Constant 5.0
    Actuator_Type 0
    Joint_Friction    0.35
}
}
Branch {
    ZScrewTxLink {
        Name "hip_screw_link"
        ZScrew_Parameters 0 1.57
    }
}
RevoluteLink {
    Name "Waist1"
    Graphics_Model "Graphics//waist2.wrl"
    Mass 1.948000
    Inertia    0.028552 -0.000003 0.000095
              -0.000003 0.027092 0.000590
              0.000095 0.000590 0.003277
    Center_of_Gravity -0.000240 -0.001316 0.090517
    Number_of_Contact_Points 4
    Contact_Locations    0.097 -0.05 -0.05
                       0.097 -0.05 0.05
                       0.097 0.05 -0.05
                       0.097 0.05 0.05
    MDH_Parameters    0 1.57 0.067 0.00
    Initial_Joint_Velocity 0.0
    Joint_Limits    -3.1416 3.1416
    Joint_Limit_Spring_Constant 50.0
    Joint_Limit_Damper_Constant 5.0
    Actuator_Type 1
    Motor_Torque_Constant 5
    Motor_BackEMF_Constant 7.02
    Motor_Armature_Resistance 1.71
    Motor_Inertia .111
    Motor_Coulomb_Friction_Constant 0.445
    Motor_Viscous_Friction_Constant 1.15
    Motor_Max_Brush_Drop 0
    Motor_Half_Drop_Value 1
}
}
ZScrewTxLink {
    Name "hip_screw_link"
    ZScrew_Parameters 0.229 0
}
}
RevoluteLink {
    Name "Waist2"
    Graphics_Model "Graphics//waist1.wrl"
    Mass 1.491000
    Inertia    0.005068 0.000152 -0.000050
              0.000152 0.006666 0.000005
              -0.000050 0.000005 0.003600
    Center_of_Gravity 0.000673 -0.013224 0.007095
    Number_of_Contact_Points 4
    Contact_Locations    0.075 -0.05 -0.05
                       0.075 -0.05 0.05
                       0.075 0.05 -0.05
                       0.075 0.05 0.05
    MDH_Parameters    0.0 -1.57 0.00 0.0
    Initial_Joint_Velocity 0.0
    Joint_Limits    -3.1416 3.1416
    Joint_Limit_Spring_Constant 50.0
    Joint_Limit_Damper_Constant 5.0
    Actuator_Type 1
}
}

```

```

    Motor_Torque_Constant 5
    Motor_BackEMF_Constant 7.02
    Motor_Armature_Resistance 1.71
    Motor_Inertia .111
    Motor_Coulomb_Friction_Constant 0.445
    Motor_Viscous_Friction_Constant 1.15
    Motor_Max_Brush_Drop 0
    Motor_Half_Drop_Value 1
}

ZScrewTxLink {                                #hip screw          9
    Name "hip_screw_link"
    ZScrew_Parameters 0.0 1.57
}

RevoluteLink {                                #Hip                  10
    Name "Hip"
    Graphics_Model "Graphics/hip_2.wrl"
    Mass 3.793000
    Inertia 0.027564 -0.001067 0.000024
            -0.001067 0.028275 0.000040
            0.000024 0.000040 0.018381
    Center_of_Gravity -0.041649 -0.004860 -0.002231
    Number_of_Contact_Points 8
    Contact_Locations -0.085 0.05 -0.085
                    -0.085 0.05 0.085
                    0.085 0.05 -0.085
                    0.085 0.05 0.085
                    -0.085 0.00 -0.085
                    -0.085 0.00 0.085
                    0.085 0.00 -0.085
                    0.085 0.00 0.085
    MDH_Parameters -0.07 1.57 0.0 0
    Initial_Joint_Velocity 0.0
    Joint_Limits -3.1416 3.1416
    Joint_Limit_Spring_Constant 50.0
    Joint_Limit_Damper_Constant 5.0
    Actuator_Type 1
    Motor_Torque_Constant 5
    Motor_BackEMF_Constant 7.02
    Motor_Armature_Resistance 1.71
    Motor_Inertia .111
    Motor_Coulomb_Friction_Constant 0.445
    Motor_Viscous_Friction_Constant 1.15
    Motor_Max_Brush_Drop 0
    Motor_Half_Drop_Value 1
}

## The dude *will* walk ##
#####
## Right Leg ##
#####

Branch {
    ZScrewTxLink {                                #Screw link          11
        Name "right_vert_rotation_screw_link"
        ZScrew_Parameters 0.075 3.14
    }

    RevoluteLink {                                #right Hip Abduction 12
        Name "right_hip_abduction"
        Graphics_Model "Graphics/abduction.wrl"
        Mass 1.518000
        Inertia 0.008775 0.003478 -0.000123
                0.003478 0.009715 0.000030
                -0.000123 0.000030 0.012664
        Center_of_Gravity 0.063097 -0.034883 -0.000866
        Number_of_Contact_Points 4
        Contact_Locations 0.157 -0.05 -0.05
                        0.157 -0.05 0.05
                        0.157 0.05 -0.05
                        0.157 0.05 0.05
        MDH_Parameters 0.06 -1.57 0 0
        Initial_Joint_Velocity 0.0
        Joint_Limits -0.1745 -0.1745
        Joint_Limit_Spring_Constant 33.105
        Joint_Limit_Damper_Constant 0.0
        Actuator_Type 1
        Motor_Torque_Constant 5
        Motor_BackEMF_Constant 7.02
        Motor_Armature_Resistance 1.71
        Motor_Inertia .111
        Motor_Coulomb_Friction_Constant 0.445
        Motor_Viscous_Friction_Constant 1.15
        Motor_Max_Brush_Drop 0
        Motor_Half_Drop_Value 1
    }

    RevoluteLink {                                #right Hip Flexion  13
        Name "right_hip_flexion"
    }
}

```

```

Graphics_Model "Graphics//flexion_right.wrl"
Mass 0.871000
Inertia    0.002735 -0.000008 -0.000544
           -0.000008 0.004637 -0.000002
           -0.000544 -0.000002 0.002661
Center_of_Gravity 0.047940 0.000185 0.013011
Number_of_Contact_Points    4
Contact_Locations    0.052 -0.05 -0.05
                    0.052 -0.05 0.05
                    0.052 0.05 -0.05
                    0.052 0.05 0.05
MDH_Parameters    0.075 1.57 0.0 0.0
Initial_Joint_Velocity 0.0
Joint_Limits    -3.1416 3.1416
Joint_Limit_Spring_Constant 50.0
Joint_Limit_Damper_Constant 5.0
Actuator_Type 1
Motor_Torque_Constant 5
Motor_BackEMF_Constant 7.02
Motor_Armature_Resistance 1.71
Motor_Inertia .111
Motor_Coulomb_Friction_Constant 0.445
Motor_Viscous_Friction_Constant 1.15
Motor_Max_Brush_Drop 0
Motor_Half_Drop_Value 1
}

ZScrewTxLink {                                #right Z screw    14
  Name "right_screw_link"
  ZScrew_Parameters    0.0 1.57
}

RevoluteLink {                                #right upper leg    15
  Name "right_Upper_leg"
  Graphics_Model "Graphics//upperleg_right.wrl"
  Mass 3.194000
  Inertia    0.072575 -0.000561 -0.000906
             -0.000561 0.065655 -0.009989
             -0.000906 -0.009989 0.010428
  Center_of_Gravity 0.004145 0.021490 0.117430
  Number_of_Contact_Points    4
  Contact_Locations    -0.05 -0.05 0.165
                     -0.05 0.05 0.165
                     0.05 -0.05 0.165
                     0.05 0.05 0.165
  MDH_Parameters    0 1.57 0.055 0.0
  Initial_Joint_Velocity 0.0
  Joint_Limits    -3.1416 3.1416
  Joint_Limit_Spring_Constant 50.0
  Joint_Limit_Damper_Constant 5.0
  Actuator_Type 1
  Motor_Torque_Constant 5
  Motor_BackEMF_Constant 7.02
  Motor_Armature_Resistance 1.71
  Motor_Inertia .111
  Motor_Coulomb_Friction_Constant 0.445
  Motor_Viscous_Friction_Constant 1.15
  Motor_Max_Brush_Drop 0
  Motor_Half_Drop_Value 1
}

ZScrewTxLink {                                #right Z screw    16
  Name "right_screw_link"
  ZScrew_Parameters    0.21 1.57
}

ZScrewTxLink {                                #right Z screw    17
  Name "right_screw_link"
  ZScrew_Parameters    0 -1.57
}

RevoluteLink {                                #right lower leg    18
  Name "right_Lower_leg"
  Graphics_Model "Graphics//lowerleg_right.wrl"
  Mass 1.719000
  Inertia    0.008714 0.000881 0.007659
             0.000881 0.043280 -0.000502
             0.007659 -0.000502 0.036357
  Center_of_Gravity 0.132869 -0.007182 -0.033632
  Number_of_Contact_Points    4
  Contact_Locations    0.183 -0.05 -0.05
                     0.183 -0.05 0.05
                     0.183 0.05 -0.05
                     0.183 0.05 0.05
  MDH_Parameters    0 1.57 0 1.57
  Initial_Joint_Velocity 0.0
  Joint_Limits    -3.57 3.1416
  Joint_Limit_Spring_Constant 50.0
  Joint_Limit_Damper_Constant 5.0
  Actuator_Type 1
  Motor_Torque_Constant 5
}

```

```

Motor_BackEMF_Constant 7.02
Motor_Armature_Resistance 1.71
Motor_Inertia .111
Motor_Coulomb_Friction_Constant 0.445
Motor_Viscous_Friction_Constant 1.15
Motor_Max_Brush_Drop 0
Motor_Half_Drop_Value 1
}

RevoluteLink {                                #right Ankle One    19
  Name "right_Ankle_One"
  Graphics_Model "Graphics//ankle_right.wrl"
  Mass 1.480000
  Inertia    0.006200 -0.001198 -0.000354
             -0.001198 0.006656 0.000004
             -0.000354 0.000004 0.007328
  Center_of_Gravity 0.046567 0.016788 0.009632
  Number_of_Contact_Points 4
  Contact_Locations 0.051 -0.05 -0.05
                   0.051 -0.05 0.05
                   0.051 0.05 -0.05
                   0.051 0.05 0.05
  MDH_Parameters 0.172 3.14 0 0.0
  Initial_Joint_Velocity 0.0
  Joint_Limits -3.1416 3.1416
  Joint_Limit_Spring_Constant 50.0
  Joint_Limit_Damper_Constant 5.0
  Actuator_Type 1
  Motor_Torque_Constant 5
  Motor_BackEMF_Constant 7.02
  Motor_Armature_Resistance 1.71
  Motor_Inertia .111
  Motor_Coulomb_Friction_Constant 0.445
  Motor_Viscous_Friction_Constant 1.15
  Motor_Max_Brush_Drop 0
  Motor_Half_Drop_Value 1
}

RevoluteLink {                                #right Foot    20
  Name "right_Foot"
  Graphics_Model "Graphics//rightfoot.wrl"
  Mass 1.149000
  Inertia    0.006964 -0.000800 0.001018
             -0.000800 0.005868 0.000842
             0.001018 0.000842 0.004083
  Center_of_Gravity 0.021083 0.020701 -0.041544
  Number_of_Contact_Points 4
  Contact_Locations 0.055 0.050 0.055
                   0.055 0.050 -0.145
                   0.055 -0.1 -0.145
                   0.055 -0.1 0.055
  MDH_Parameters 0.051 1.57 0.0 0.0
  Initial_Joint_Velocity 0.0
  Joint_Limits 3.1745 -3.1745
  Joint_Limit_Spring_Constant 33.105
  Joint_Limit_Damper_Constant 0.0
  Actuator_Type 1
  Motor_Torque_Constant 5
  Motor_BackEMF_Constant 7.02
  Motor_Armature_Resistance 1.71
  Motor_Inertia .111
  Motor_Coulomb_Friction_Constant 0.445
  Motor_Viscous_Friction_Constant 1.15
  Motor_Max_Brush_Drop 0
  Motor_Half_Drop_Value 1
}

}

#####
## Left Leg ##
#####
Branch {
  ZScrewTxLink {                                #left Screw    21
    Name "left_vert_rotation_screw_link"
    ZScrew_Parameters -0.075 3.14
  }

  RevoluteLink {                                #left Hip Adduction 22
    Name "left_hip_abduction"
    Graphics_Model "Graphics//abduction.wrl"
    Mass 1.510000
    Inertia    0.008702 0.003510 0.000096
               0.003510 0.009679 -0.000043
               0.000096 -0.000043 0.012706
    Center_of_Gravity 0.063625 -0.035371 0.001644
    Number_of_Contact_Points 4
    Contact_Locations 0.157 -0.05 -0.05
                     0.157 -0.05 0.05
                     0.157 0.05 -0.05
  }
}

```



```

MDH_Parameters          0.157 0.05 0.05
Initial_Joint_Velocity  0.06 1.57 0.0 0
Joint_Limits            -0.1745 -0.1745
Joint_Limit_Spring_Constant 33.105
Joint_Limit_Damper_Constant 0.0
Actuator_Type 1
Motor_Torque_Constant 5
Motor_BackEMF_Constant 7.02
Motor_Armature_Resistance 1.71
Motor_Inertia .111
Motor_Coulomb_Friction_Constant 0.445
Motor_Viscous_Friction_Constant 1.15
Motor_Max_Brush_Drop 0
Motor_Half_Drop_Value 1
}

RevoluteLink { #left hip flexion 23
  Name "left_hip_flexion"
  Graphics_Model "Graphics//flexion_left.wrl"
  Mass 0.871000
  Inertia 0.002737 -0.000023 0.000547
          -0.000023 0.004647 0.000006
          0.000547 0.000006 0.002671
  Center_of_Gravity 0.048050 0.000554 -0.013069
  Number_of_Contact_Points 4
  Contact_Locations 0.052 -0.05 -0.05
                   0.052 -0.05 0.05
                   0.052 0.05 -0.05
                   0.052 0.05 0.05
  MDH_Parameters 0.075 -1.57 0.0 0.0
  Initial_Joint_Velocity 0.0
  Joint_Limits -3.1416 3.1416
  Joint_Limit_Spring_Constant 50.0
  Joint_Limit_Damper_Constant 5.0
  Actuator_Type 1
  Motor_Torque_Constant 5
  Motor_BackEMF_Constant 7.02
  Motor_Armature_Resistance 1.71
  Motor_Inertia .111
  Motor_Coulomb_Friction_Constant 0.445
  Motor_Viscous_Friction_Constant 1.15
  Motor_Max_Brush_Drop 0
  Motor_Half_Drop_Value 1
}

ZScrewTxLink { #left Z screw 24
  Name "left_screw_link"
  ZScrew_Parameters 0.0 1.57
}

RevoluteLink { #left upper leg 25
  Name "left_Upper_leg"
  Graphics_Model "Graphics//upperleg_left.wrl"
  Mass 3.193000
  Inertia 0.073221 0.001330 -0.003409
          0.001330 0.066317 0.010776
          -0.003409 0.010776 0.011285
  Center_of_Gravity 0.009504 -0.023414 0.117745
  Number_of_Contact_Points 4
  Contact_Locations -0.05 -0.05 0.165
                   -0.05 0.05 0.165
                   0.05 -0.05 0.165
                   0.05 0.05 0.165
  MDH_Parameters 0.0 1.57 0.055 0.0
  Initial_Joint_Velocity 0.0
  Joint_Limits -3.1416 3.1416
  Joint_Limit_Spring_Constant 50.0
  Joint_Limit_Damper_Constant 5.0
  Actuator_Type 1
  Motor_Torque_Constant 5
  Motor_BackEMF_Constant 7.02
  Motor_Armature_Resistance 1.71
  Motor_Inertia .111
  Motor_Coulomb_Friction_Constant 0.445
  Motor_Viscous_Friction_Constant 1.15
  Motor_Max_Brush_Drop 0
  Motor_Half_Drop_Value 1
}

ZScrewTxLink { #Left Z screw 26
  Name "left_screw_link"
  ZScrew_Parameters 0.21 1.57
}

ZScrewTxLink { #Left Z screw 27
  Name "left_screw_link"
  ZScrew_Parameters 0 -1.57
}

RevoluteLink { #left lower leg 28

```



```

## Right Arm ##
#####
Branch {
  RevoluteLink {
    Name "Right_Shoulder"
    Graphics_Model "Graphics//shoulder_right.wrl"
    Mass 0.202000
    Inertia 0.000186 0.000030 -0.000071
            0.000030 0.000245 0.000040
            -0.000071 0.000040 0.000215
    Center_of_Gravity 0.017956 -0.007800 0.020045
    Number_of_Contact_Points 4
    Contact_Locations 0.00 -0.025 -0.025
                    0.00 -0.025 0.025
                    0.00 0.025 -0.025
                    0.00 0.025 0.025
    MDH_Parameters 0.03 -1.57 0.21 0.00
    Initial_Joint_Velocity 0.0
    Joint_Limits -3.1416 3.1416
    Joint_Limit_Spring_Constant 50.0
    Joint_Limit_Damper_Constant 5.0
    Actuator_Type 0
    Joint_Friction 0.35
  }

  ZScrewTxLink {
    Name "right_screw_link"
    ZScrew_Parameters 0.024 1.57
  }

  ZScrewTxLink {
    Name "right_screw_link"
    ZScrew_Parameters 0 -1.57
  }

  RevoluteLink {
    Name "Right_Upper_Arm"
    Graphics_Model "Graphics//upperarm.wrl"
    Mass 0.377000
    Inertia 0.000424 -0.000339 0.000221
            -0.000339 0.011035 0.000006
            0.000221 0.000006 0.010903
    Center_of_Gravity 0.155219 0.004800 -0.004078
    Number_of_Contact_Points 4
    Contact_Locations 0.22 -0.025 -0.025
                    0.22 -0.025 0.025
                    0.22 0.025 -0.025
                    0.22 0.025 0.025
    MDH_Parameters 0.0 1.57 0.0 0.0
    Initial_Joint_Velocity 0.0
    Joint_Limits -3.1416 3.1416
    Joint_Limit_Spring_Constant 50.0
    Joint_Limit_Damper_Constant 5.0
    Actuator_Type 0
    Joint_Friction 0.35
  }

  RevoluteLink {
    Name "Right_Lower_Arm"
    Graphics_Model "Graphics//lowerarm.wrl"
    Mass 0.328000
    Inertia 0.000395 -0.000004 0.000013
            -0.000004 0.004837 0.000000
            0.000013 0.000000 0.004715
    Center_of_Gravity 0.102913 0.000121 -0.001362
    Number_of_Contact_Points 4
    Contact_Locations 0.245 -0.025 -0.025
                    0.245 -0.025 0.025
                    0.245 0.025 -0.025
                    0.245 0.025 0.025
    MDH_Parameters 0.209 -1.57 0.00 0.0
    Initial_Joint_Velocity 0.0
    Joint_Limits -3.1416 3.1416
    Joint_Limit_Spring_Constant 50.0
    Joint_Limit_Damper_Constant 5.0
    Actuator_Type 0
    Joint_Friction 0.35
  }
}

#####
## Left Arm ##
#####
Branch {
  RevoluteLink {
    Name "Left_Shoulder"
    Graphics_Model "Graphics//shoulder_left.wrl"
    Mass 0.206000
    Inertia 0.000190 0.000026 0.000063
            0.000026 0.000237 -0.000039
  }
}

```


Appendix B

Motor / Gearhead Characteristic Spreadsheet

This Spread sheet was used to quickly evaluate the characteristics of any particular motor and gearhead combination by entering the parameters found in the corresponding datasheet. Continuous, Maximum and Operating Point characteristics are calculated.

Motor Characteristic Calculations

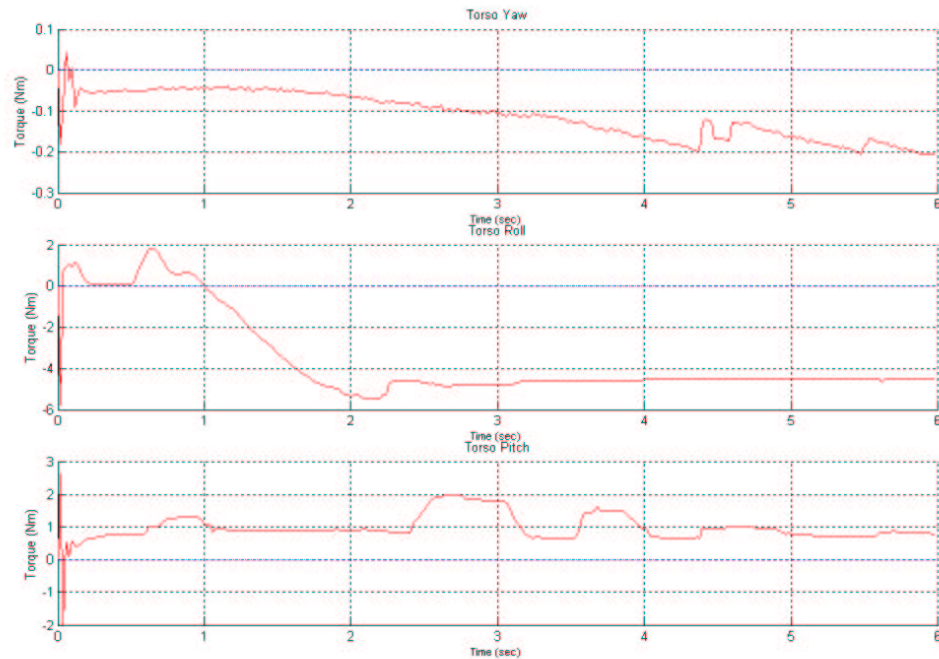
Calcs at Nominal

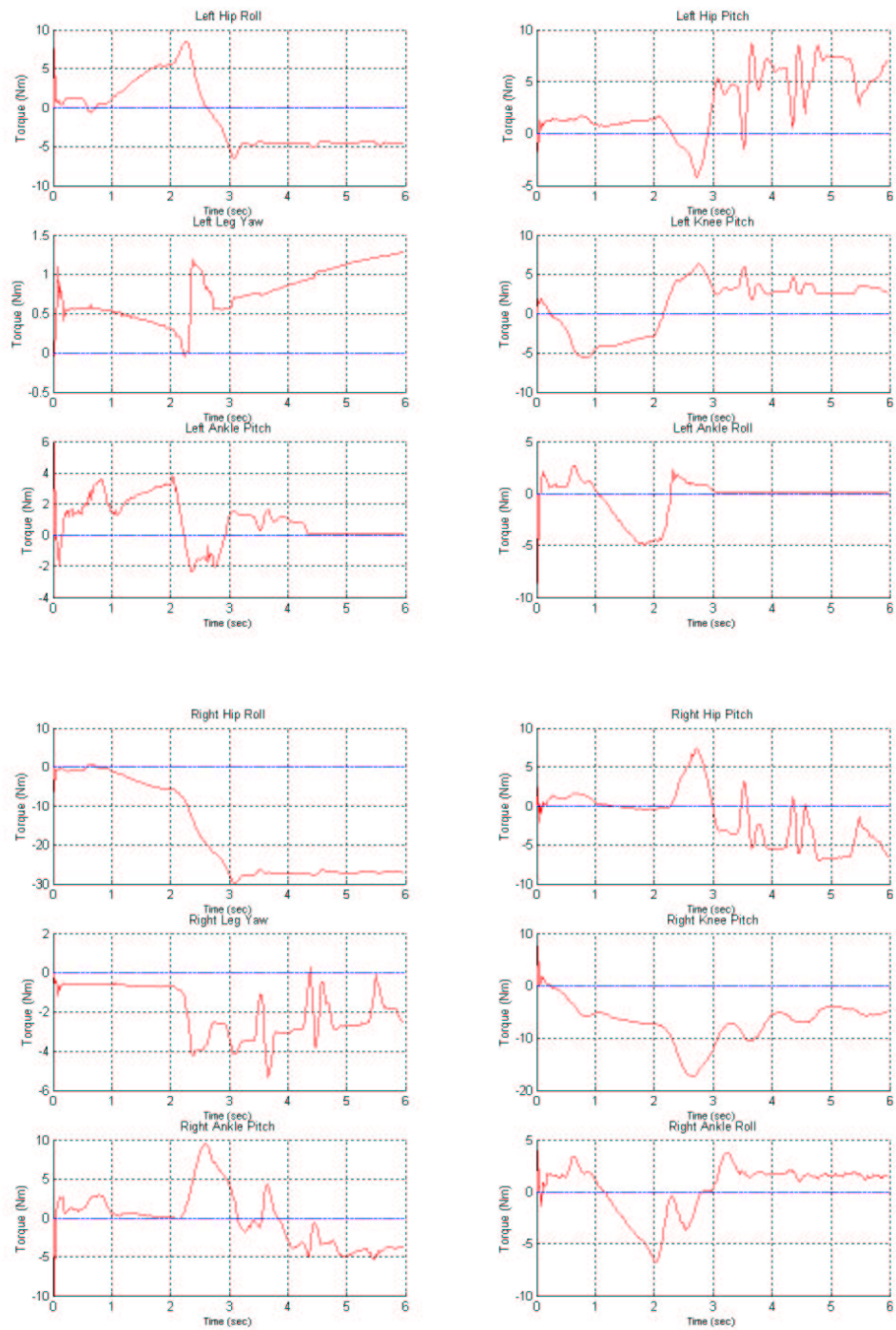
Nominal voltage	32 V	no load	6790 rpm	
max contin speed	6790 rpm	Starting current	21.5 A	
max contin torque	88.5 mNm	max permissible speed	8200 rpm	
Max mech power	146 W			
Terminal resistance	1.71 Ohm			
Stall Torque	832 mNm	Gear Ratio	156	
Current Const (Ki)	0.02	Gear Eff	0.7	
Torque Const (Km)	44.5	Max gearbox contin	15.00	
Back EMF (Ke)	0.05	Max gear output	22.50	
Rth	9.8 C/W			
Continuous		Characteristic @ operating point		
T at Gear	9.66 Nm			
w at gear	43.53 rpm	Requirements		
w at gear	4.56 rad/s	Torque Required	10 Nm	
Current	1.99 A	Speed required (rpm)	20	
		Speed	2.10 rad/s	
Maximum				
Max T at Gear	90.85 Nm	Current required	2.06 A	
Max current	18.70 A	Voltage Required	3.66 V	
		Output power	20.94 W	
		Rotor Temperature	95.97	
Max mech power	146.00 W			
Rotor temp contin	91.28 C	Power (mech)	20.97 W	
current for max gearbox	4.63 A	Power lost	6.29 W	
rotor temp max gearbox	384.27 C			
		Tf (torque lost to friction)	3.00	
Torque provided at 4A	19.44 A	motor friction	1.43	

Appendix C

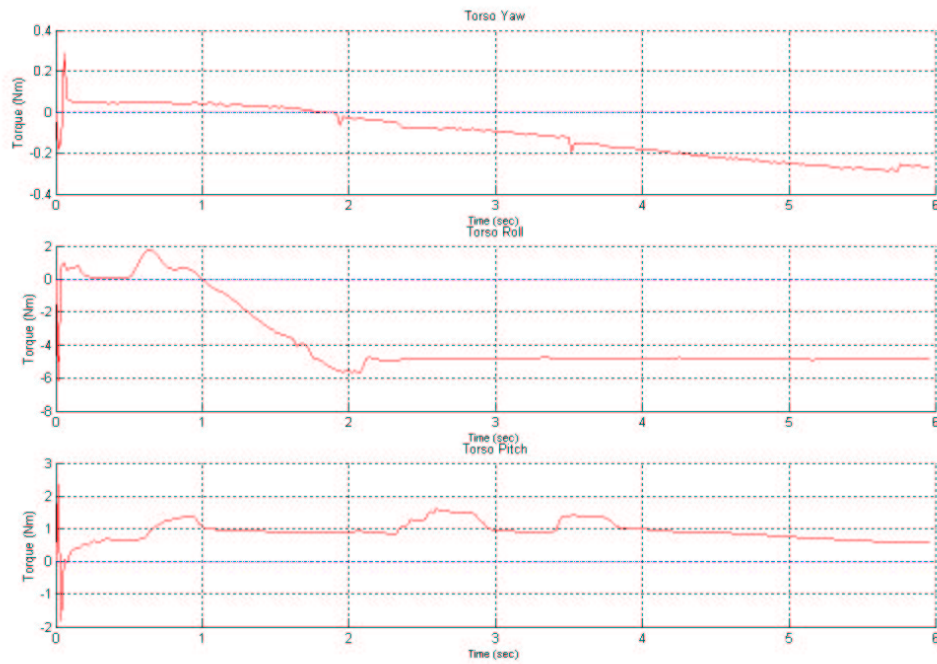
Standing on One Leg Graphs

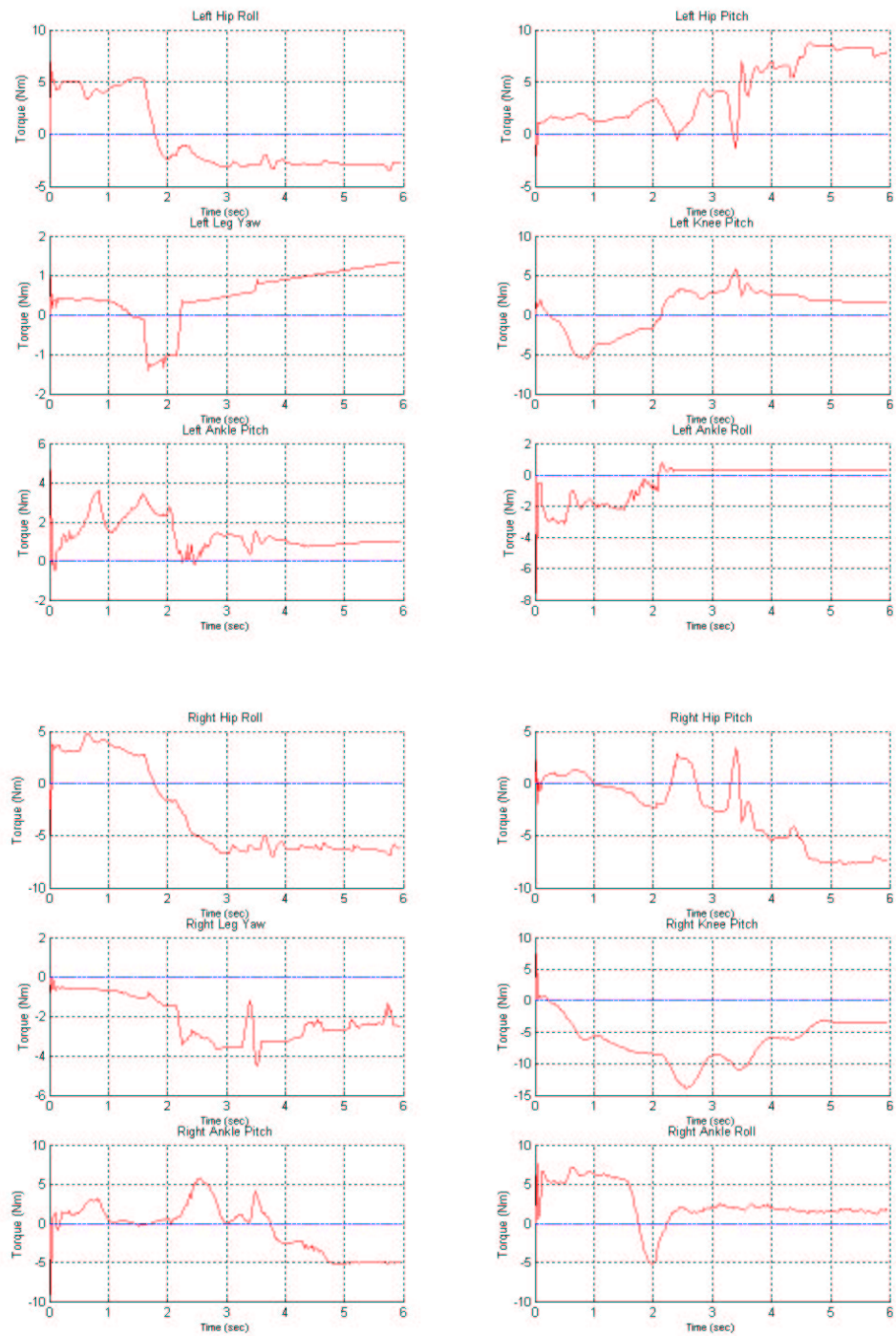
These figures graph the torque acting on each of the 15 brushed DC motors in the lower body. Analysis of these results can be found in Section 6.2.





The same movement as Section 6.2 was conducted with a set of torsional springs assisting the Hip Roll motors. Analysis of these results can be found in Section 6.5.

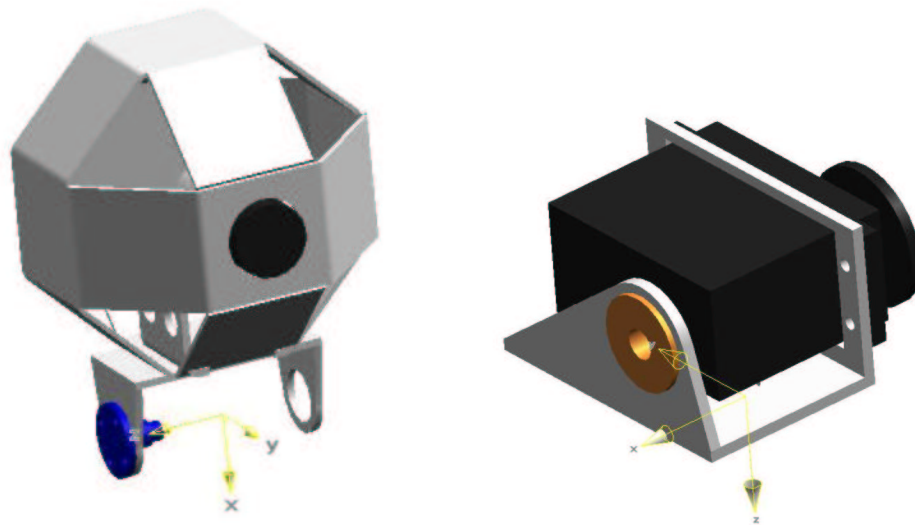


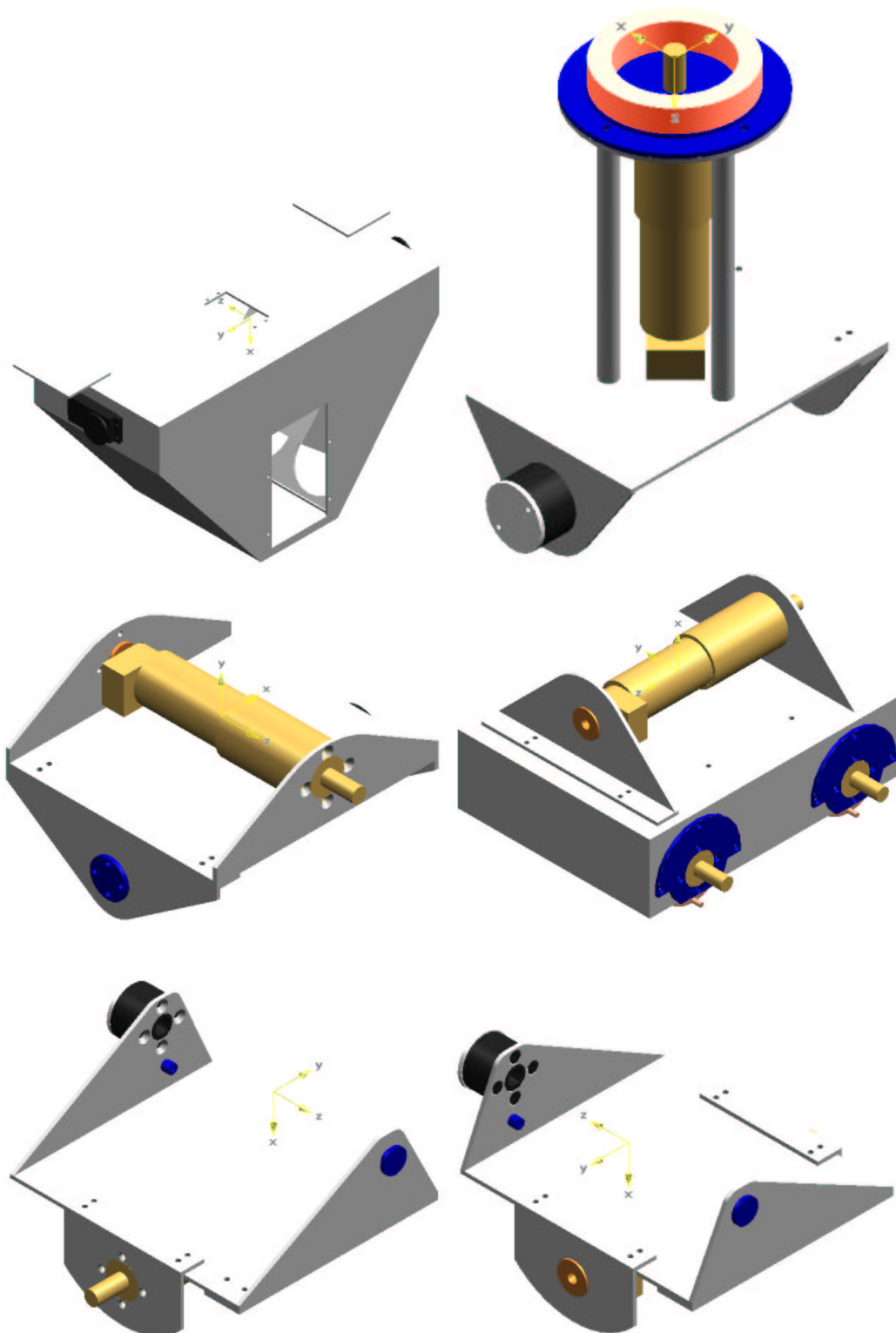


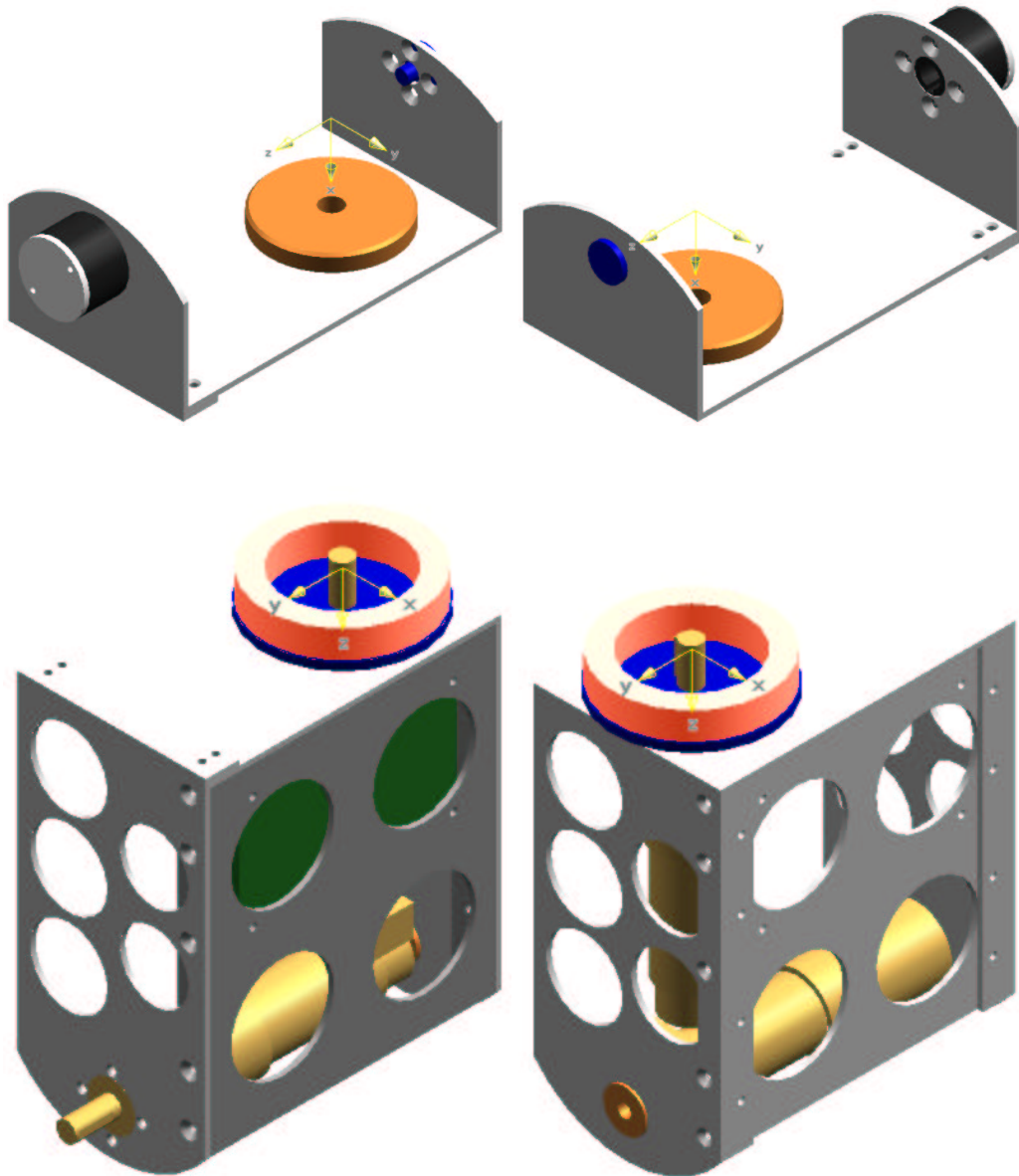
Appendix D

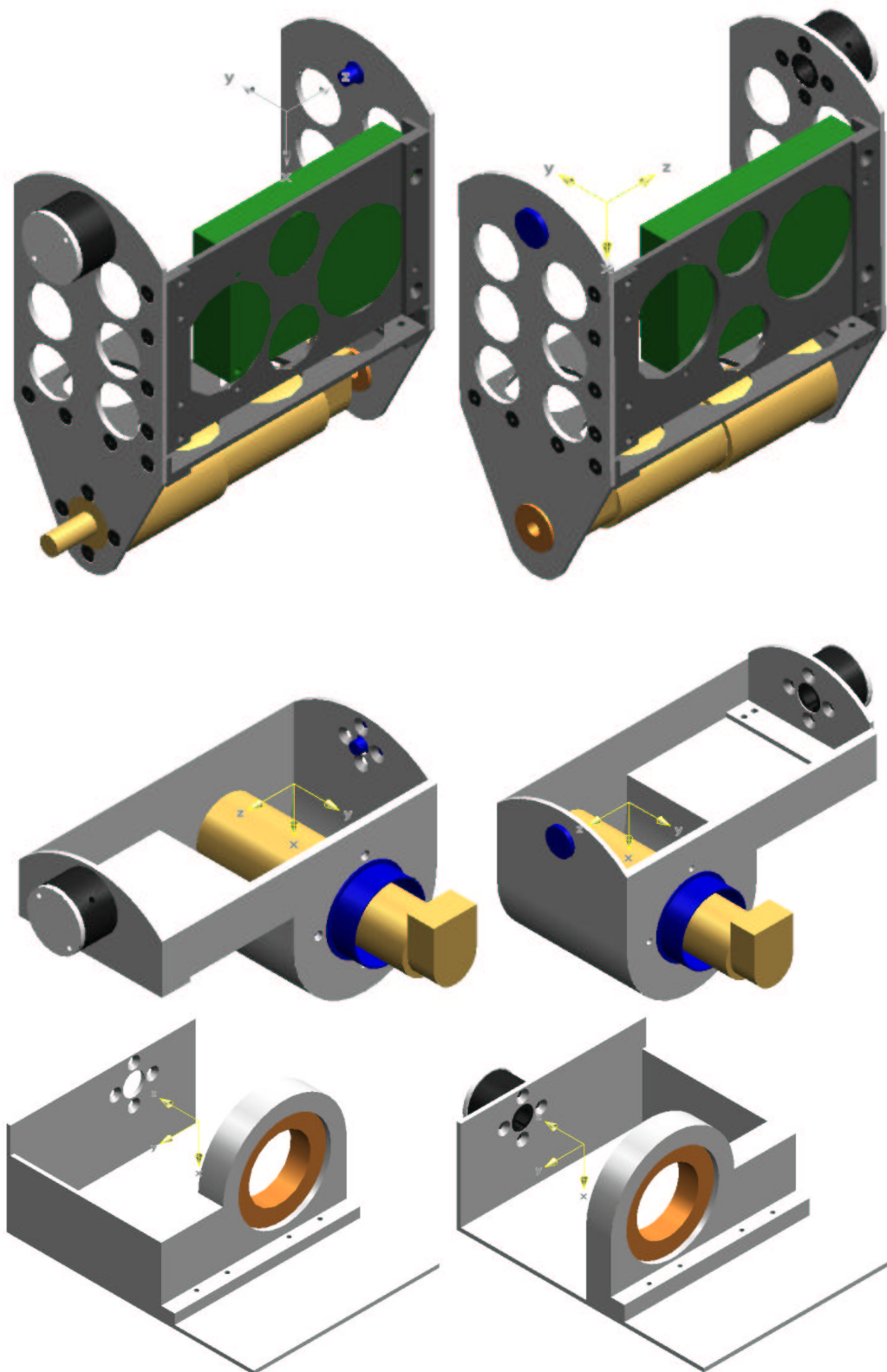
Coordinate Frames

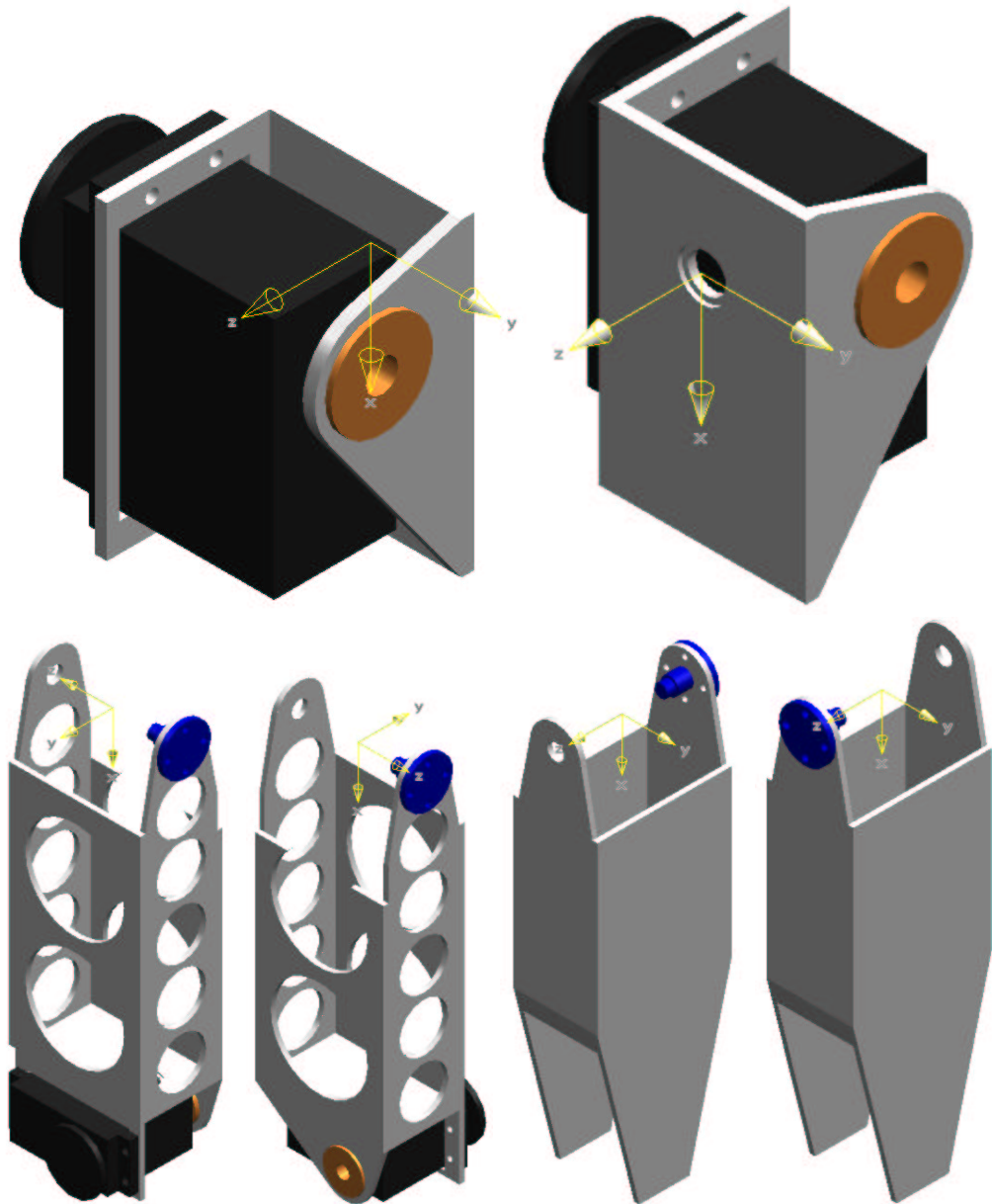
Each link has a coordinate frame associated with it. This coordinate frame is used to calculate the inertia tensor and centre of gravity for the link. The coordinate frame is also used to orientate the graphics models used in the simulator.











Appendix E

Maxon Datasheets

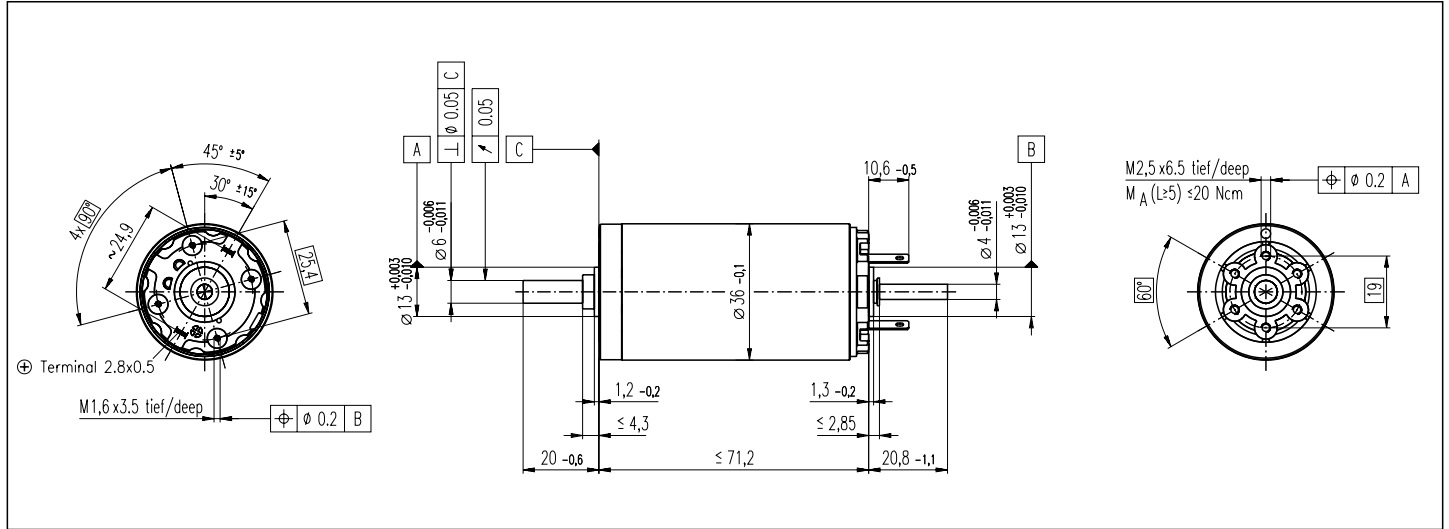
Motor: RE36 70W Brushed DC motor

Gearhead: 156:1, 3 Stage, Ceramic Planetary Gearhead

**Encoder: HEDS 0055, 500 count per revolution encoder.
2 Channels + Index Channel.**

RE 36

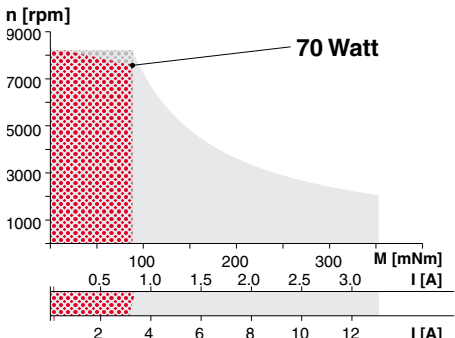
Ø36 mm, Graphite Brushes, 70 Watt



Motor Data: **Order Number**

		118797	118798	118799	118800	118801	118802	118803	118804	118805	118806	118807	118808	118809	118810
1 Assigned power rating	W	70	70	70	70	70	70	70	70	70	70	70	70	70	70
2 Nominal voltage	Volt	18.0	24.0	32.0	42.0	42.0	48.0	48.0	48.0	48.0	48.0	48.0	48.0	48.0	48.0
3 No load speed	rpm	6410	6210	6790	7020	6340	6420	5220	4320	3450	2830	2280	1780	1420	1180
4 Stall torque	mNm	730	783	832	865	786	785	627	504	403	326	258	198	158	127
5 Speed/torque gradient	rpm/mNm	8.96	8.05	8.27	8.19	8.14	8.25	8.41	8.65	8.67	8.80	8.96	9.17	9.21	9.51
6 No load current	mA	147	105	89	70	61	55	42	33	25	20	15	12	9	7
7 Starting current	A	27.8	21.5	18.7	15.3	12.6	11.1	7.22	4.80	3.06	2.04	1.30	0.784	0.501	0.334
8 Terminal resistance	Ohm	0.647	1.11	1.71	2.75	3.35	4.32	6.65	10.00	15.7	23.5	36.8	61.3	95.8	144
9 Max. permissible speed	rpm	8200	8200	8200	8200	8200	8200	8200	8200	8200	8200	8200	8200	8200	8200
10 Max. continuous current	A	3.14	2.44	1.99	1.59	1.44	1.27	1.03	0.847	0.679	0.556	0.445	0.346	0.277	0.226
11 Max. continuous torque	mNm	82.4	88.8	88.5	89.8	90.4	90.1	89.8	89.0	89.2	88.8	88.1	87.3	87.2	85.8
12 Max. power output at nominal voltage	W	119	125	146	157	129	131	84.9	56.4	36.0	23.9	15.2	9.09	5.78	3.82
13 Max. efficiency	%	84	85	86	86	86	86	85	84	82	81	79	77	75	72
14 Torque constant	mNm/A	26.3	36.4	44.5	56.6	62.6	70.7	86.9	105	131	160	198	253	315	380
15 Speed constant	rpm/V	364	263	215	169	152	135	110	90.9	72.7	59.8	48.2	37.8	30.3	25.1
16 Mechanical time constant	ms	6	6	6	6	6	6	6	6	6	6	6	6	6	6
17 Rotor inertia	gcm ²	62.0	67.7	65.2	65.4	65.6	64.6	63.3	61.5	61.3	60.3	59.2	57.8	57.5	55.7
18 Terminal inductance	mH	0.10	0.20	0.30	0.49	0.60	0.76	1.15	1.68	2.62	3.87	5.96	9.70	15.10	21.90
19 Thermal resistance housing-ambient	K/W	6.4	6.4	6.4	6.4	6.4	6.4	6.4	6.4	6.4	6.4	6.4	6.4	6.4	6.4
20 Thermal resistance rotor-housing	K/W	3.4	3.4	3.4	3.4	3.4	3.4	3.4	3.4	3.4	3.4	3.4	3.4	3.4	3.4
21 Thermal time constant winding	s	39	43	41	41	41	41	40	39	39	38	37	36	36	35

Operating Range **Comments** [Details on page 36](#)



Recommended operating range
 Continuous operation
 In observation of above listed thermal resistances (lines 19 and 20) the maximum permissible rotor temperature will be reached during continuous operation at 25°C ambient. = Thermal limit.
 Short term operation
 The motor may be briefly overloaded (recurring).

118804 Motor with high resistance winding
118797 Motor with low resistance winding

Stock program
Standard program
Special program (on request!)

- Axial play 0.05 - 0.15 mm
 - Max. ball bearing loads
 - axial (dynamic) not preloaded 5.6 N
 - preloaded 2.4 N
 - radial (5 mm from flange) 28 N
 - Press-fit force (static) 110 N
 - same as above, shaft supported 1200 N
 - Radial play ball bearings 0.025 mm
 - Ambient temperature range -20/+100°C
 - Max. rotor temperature +125°C
 - Number of commutator segments 13
 - Weight of motor 350 g
 - Values listed in the table are nominal. For applicable tolerances (see page 33) and additional details please request our computer printout.
- ⚠ Tolerances may vary from the standard specification.

maxon Modular System

Planetary Gearhead
 Ø32 mm
 0.75-4.5 Nm
 Details page 161

Planetary Gearhead
 Ø32 mm
 0.4-2 Nm
 Details page 163

Planetary Gearhead
 Ø42 mm
 3-15 Nm
 Details page 165

DC Tacho
 Ø22 mm
 0.52 V
 Details page 172

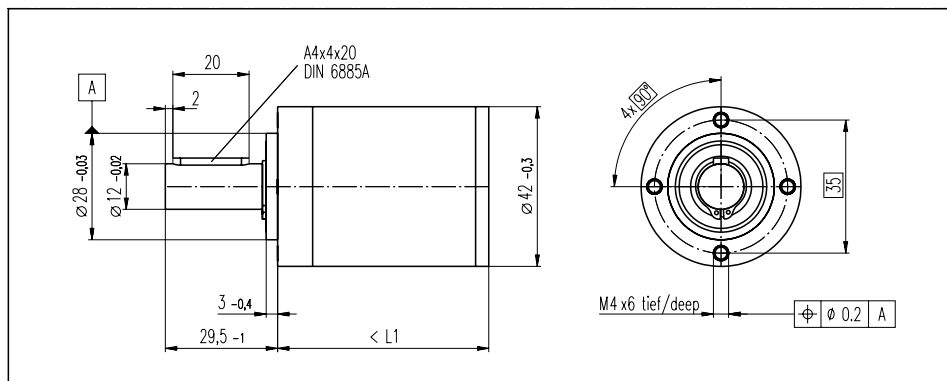
Digital Encoder HP HEDS 5540
 500 CTP, 3 channels
 Details page 176

Digital Encoder HP HEDL 5540
 500 CTP, 3 channels
 Details page 178

CERAMICVERSION

NEW

Planetary Gearhead GP 42
 Ø42 mm, 3-15 Nm



Technical Data

Planetary Gearhead	straight teeth
Output shaft	stainless steel
Bearing at output	ball bearings
Radial play, 12 mm from flange	preloaded
Axial play	preloaded
Max. permissible axial load	150 N
Max. permissible force for press fits	300 N
Recommended input speed	< 8000 rpm
Recommended temperature range	-20/+100°C
Number of stages	1 2 3 4
Max. perm. radial load, 12 mm from flange	120 N 150 N 150 N 150 N

Gearhead Data:

Order number	203113	203115	203120	203125	203128	203134	203139
1 Reduction	3.5 : 1	12 : 1	43 : 1	91 : 1	150 : 1	319 : 1	546 : 1
2 Reduction absolute	7/2	49/4	343/8	91	2401/16	637/2	546
Order number	203114	203116	203121	203126	203130	203135	203140
1 Reduction	4.3 : 1	15 : 1	53 : 1	113 : 1	186 : 1	353 : 1	676 : 1
2 Reduction absolute	13/3	91/6	637/12	338/3	4459/24	28561/81	676
Order number	203117	203122	203127	203131	203136	203141	
1 Reduction	19 : 1	66 : 1	126 : 1	230 : 1	394 : 1	756 : 1	
2 Reduction absolute	169/9	1183/18	126	8281/36	1183/3	756	
Order number	203118	203123	203129	203132	203137	203142	
1 Reduction	21 : 1	74 : 1	156 : 1	257 : 1	441 : 1	936 : 1	
2 Reduction absolute	21	147/2	156	1029/4	441	936	
Order number	203119	203124	203133	203138			
1 Reduction	26 : 1	81 : 1	285 : 1	488 : 1			
2 Reduction absolute	26	2197/27	15379/54	4394/9			
3 Number of stages	1	2	3	4	4	4	
4 Max. continuous torque at gear output	Nm 3.0	7.5	15	15	15	15	
5 Intermittently permissible torque at gear output	Nm 4.5	11.25	22.5	22.5	22.5	22.5	
6 Sense of rotation, drive to output	=	=	=	=	=	=	
7 Max. efficiency	% 90	81	72	72	64	64	
8 Weight	g 260	360	460	460	560	560	
9 Gearhead length L1	mm 41.0	55.5	70.0	70.0	84.5	84.5	

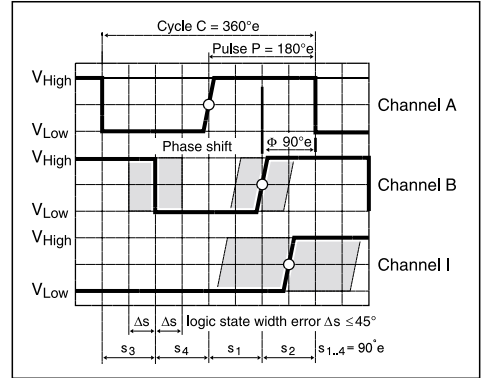
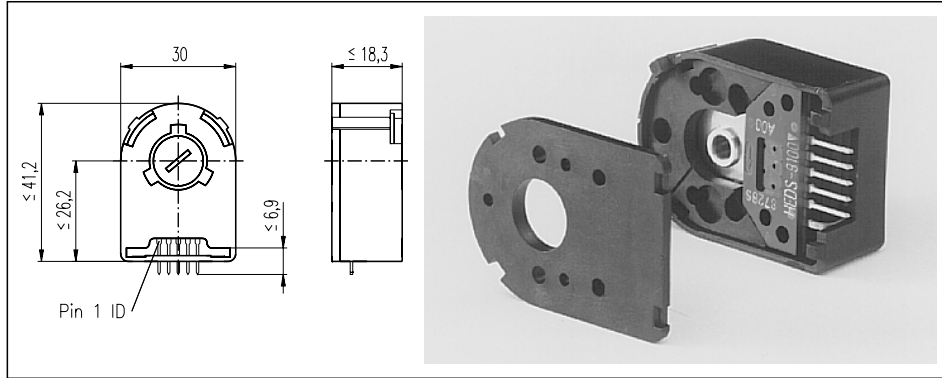


Stock program
 Standard program
 Special program (on request!)

Combination:

+ Motor	Page	+ Tacho	Page	+ Brake	Page	Overall length [mm]						
RE 35, 90 W	63					112.0	126.5	141.0	141.0	155.5	155.5	155.5
RE 35, 90 W	63	DC-Tacho 22	172			130.1	144.6	159.1	159.1	173.6	173.6	173.6
RE 35, 90 W	63	Digital Encoder HED_55_	176/178			133.0	147.5	162.0	162.0	176.5	176.5	176.5
RE 36, 70 W	64					112.3	126.8	141.3	141.3	155.8	155.8	155.8
RE 36, 70 W	64	DC-Tacho 22	172			130.4	144.9	159.4	159.4	173.9	173.9	173.9
RE 36, 70 W	64	Digital Encoder HED_55_	176/178			132.3	146.8	161.3	161.3	175.8	175.8	175.8
RE 40, 150 W	65					112.1	126.6	141.1	141.1	155.6	155.6	155.6
RE 40, 150 W	65	Digital Encoder HEDL_91_	180			132.8	147.3	161.8	161.8	176.3	176.3	176.3
RE 40, 150 W	65	Digital Encoder HEDL_91_	180			158.9	173.4	187.9	187.9	202.4	202.4	202.4
RE 40, 150 W	65			Brake 28	188	174.5	189.0	203.5	203.5	218.0	218.0	218.0
RE 40, 150 W	65			Brake 28	188	158.9	173.4	187.9	187.9	202.4	202.4	202.4
EC 40, 120 W	129					111.1	125.6	140.1	140.1	154.6	154.6	154.6
EC 40, 120 W	129	Digital Encoder HED_55_	177/179			129.5	144.0	158.5	158.5	173.0	173.0	173.0
EC 40, 120 W	129	Resolver 26	185			137.7	152.2	166.7	166.7	181.2	181.2	181.2
EC 45, 150 W	130					152.3	166.8	181.3	181.3	195.8	195.8	195.8
EC 45, 150 W	130	Digital Encoder HEDL_91_	180			167.9	182.4	196.9	196.9	211.4	211.4	211.4
EC 45, 150 W	130	Digital Encoder HEDL_91_	180	Brake 28	188	167.9	182.4	196.9	196.9	211.4	211.4	211.4
EC 45, 150 W	130	Resolver 26	185			152.3	166.8	181.3	181.3	195.8	195.8	195.8
EC 45, 150 W	130			Brake 28	188	167.9	182.4	196.9	196.9	211.4	211.4	211.4
EC 45, 250 W	131					185.1	199.6	214.1	214.1	228.6	228.6	228.6
EC 45, 250 W	131	Digital Encoder HEDL_91_	180			200.7	215.2	229.7	229.7	244.2	244.2	244.2
EC 45, 250 W	131	Digital Encoder HEDL_91_	180	Brake 28	188	200.7	215.2	229.7	229.7	244.2	244.2	244.2
EC 45, 250 W	131	Resolver 26	185			185.1	199.6	214.1	214.1	228.6	228.6	228.6
EC 45, 250 W	131			Brake 28	188	200.7	215.2	229.7	229.7	244.2	244.2	244.2

Digital Encoder
HEDS 55__



Type						
Order numbers	110509	110511	110513	110515	137397	
Shaft diameter	mm	2	3	4	6	8



Combination:						Overall length [mm] / ● see: + Gearhead
+ Motor	Page	+ Gearhead	Page	+ Brake	Page	
RE 25, 10 W	60					75.3
RE 25, 10 W	60	GP 26, 0.2-2.0 Nm	157/158			●
RE 25, 10 W	60	GP 32, 0.4-4.5 Nm	160/163			●
RE 25, 20 W	61					75.3
RE 25, 20 W	61	GP 26, 0.2-2.0 Nm	157/158			●
RE 25, 20 W	61	GP 32, 0.4-4.5 Nm	160/163			●
RE 26, 18 W	62					77.2
RE 26, 18 W	62	GP 26, 0.2-2.0 Nm	157/158			●
RE 26, 18 W	62	GP 32, 0.4-4.5 Nm	160/163			●
RE 35, 90 W	63					91.9
RE 35, 90 W	63	GP 32, 0.75-4.5 Nm	161			●
RE 35, 90 W	63	GP 42, 3-15 Nm	165			●
RE 36, 70 W	64					92.2
RE 36, 70 W	64	GP 32, 0.75-4.5 Nm	161			●
RE 36, 70 W	64	GP 32, 0.4-2.0 Nm	163			●
RE 36, 70 W	64	GP 42, 3-15 Nm	165			●
RE 40, 150 W	65					91.7
RE 40, 150 W	65	GP 42, 3-15 Nm	165			●
RE 75, 250 W	66					241.5
RE 75, 250 W	66	GP 81, 20-120 Nm	167			●
RE 75, 250 W	66			Brake 75	189	281.4
RE 75, 250 W	66	GP 81, 20-120 Nm	167	Brake 75	189	●
S 2322, 6 W	69					68.8
S 2322, 6 W	69	GP 22, 0.5-1.0 Nm	154			●
S 2322, 6 W	69	GP 22, 0.5-2.0 Nm	155			●
S 2322, 6 W	69	GP 26, 0.2-1.8 Nm	157			●
S 2322, 6 W	69	GP 26, 0.5-2.0 Nm	158			●
S 2326, 6 W	72					64.5
S 2326, 6 W	72	GP 26, 0.2-1.8 Nm	157			●
S 2326, 6 W	72	GS 38, 0.1-0.6 Nm	164			●

Technical Data	Pin Allocation	Test Circuit
Supply voltage: 5 V ± 10%		
Output signal: TTL compatible		
Number of channels: 2 + 1 Index channel	Cable with plug: maxon Art. Nr. 3409.506 The plug (Harting 918.906.6803) can be fixed in the required position.	Ambient temperature $\delta U = 25^\circ\text{C}$
Counts per turn: 500 1000	Cable with plug: (compatible with Encoder HEDS5010) maxon Art. Nr. 3409.504 The plug (3M 891100101) can be fixed in the required position.	
Phase shift Φ (nominal): 90°e		
Logic state width s: min. 45°e		
Signal rise time (typical at $C_L = 25\text{ pF}$, $R_L = 2.7\text{ k}\Omega$, 25°C): 180 ns		
Signal fall time (typical at $C_L = 25\text{ pF}$, $R_L = 2.7\text{ k}\Omega$, 25°C): 40 ns		
Index pulse width (nominal) Option: 90°e		
Operating temperature range: -40/+100°C		
Moment of inertia of code wheel: $\le 0.6\text{ gcm}^2$		
Max. acceleration: 250'000 rad s ⁻²		
Output current per channel: min. -1 mA, max. 5 mA		
Max. operating frequency: 100 kHz		